Atmos. Chem. Phys. Discuss., 10, 16007–16054, 2010
www.atmos-chem-phys-discuss.net/10/16007/2010/
doi:10.5194/acpd-10-16007-2010

Atmospheric Chemistry and Physics Discussions

Improvement and evaluation of simulated global biogenic soil NO emissions in an AC-GCM

J. Steinkamp[1] **and M. G. Lawrence**[1,2]

[1]Max-Planck-Institute for Chemistry, Department of Atmospheric Chemistry, Mainz, Germany
[2]University of Mainz, Institute for Physics of the Atmosphere, Mainz,Germany

Received: 27 May 2010 – Accepted: 22 June 2010 – Published: 30 June 2010

Correspondence to: J. Steinkamp (joerg.steinkamp@mpic.de)

Published by Copernicus Publications on behalf of the European Geosciences Union.

Abstract

Soil biogenic NO emissions (SNO_x) play important direct and indirect roles in chemical processes of the troposphere. The most widely applied algorithm to calculate SNO_x in global models was published 15 years ago by Yienger and Levy (1995), and was based on very few measurements. Since then numerous new measurements have been published, which we used to build up a database of field measurements conducted world wide covering the period from 1978 to 2009, including 108 publications with 560 measurements.

Recently, several satellite based top-down approaches, which recalculated the different sources of NO_x (fossil fuel, biomass burning, soil and lightning), have shown an underestimation of SNO_x by the algorithm of Yienger and Levy (1995). Nevertheless, to our knowledge no general improvements of this algorithm have yet been published.

Here we present major improvements to the algorithm, which should help to optimize the representation of SNO_x in atmospheric-chemistry global climate models, without modifying the underlying principal or mathematical equations. The changes include: 1) Using a new up to date land cover map, with twice the number of land cover classes, and using annually varying fertilizer application rates; 2) Adopting the fraction of SNO_x induced by fertilizer application based on our database; 3) Switching from soil water column to volumetric soil moisture, to distinguish between the wet and dry state; 4) Tuning the emission factors to reproduce the measured emissions in our database and calculate the emissions based on their mean value. These steps lead us to increased global yearly SNO_x, and our total SNO_x source ends up being close to one of the top-down approaches. In some geographical regions the new results agree better with the top-down approach, but there are also distinct differences in other regions. This suggests that a combination of both top-down and bottom-up approaches could be combined in a future attempt to provide an even better calculation of SNO_x.

ACPD

10, 16007–16054, 2010

1 Introduction

Nitrogen oxides (NO_x=NO+NO_2) play an important role in the chemical processes of the atmosphere, mainly in the production and destruction of ozone (Chameides et al., 1992). On a global scale NO_x emissions are dominated by anthropogenic combustion, which contributes 20–24 Tg(N) y^{-1} (Denman et al., 2007). Biogenic NO emission flux from soils (hereafter SNO_x) contributes 5.5–21 Tg(N) y^{-1} (Yienger and Levy, 1995; Davidson and Kingerlee, 1997) and is in the same range as NO produced by lightning and biomass burning. However in a previous study we could show that due to the geographical distribution of modeled SNO_x, its influence on the reaction chain from NO_x through O_3 and OH to the oxidizing efficiency is stronger than for the other surface sources (Steinkamp et al., 2009).

In recent years, measurements of the NO_2 column from satellites were used in so called top-down approaches to optimize emissions from various sources including SNO_x (Martin et al., 2003, 2006; Bertram et al., 2005; Jaeglé et al., 2005; Müller and Stavrakou, 2005). Coming from the other direction, bottom-up approaches have used various algorithms for estimating SNO_x based on soil and climatological parameters. The most widely used algorithm to calculate SNO_x was developed 15 years ago by Yienger and Levy (1995) (hereafter YL95o, "o" for original) and has been applied in numerous atmospheric chemistry global climate models (Lawrence et al., 1999; Ganzeveld et al., 2002; Horowitz et al., 2003; Martin et al., 2003; Hauglustaine et al., 2004; Jaeglé et al., 2005; Müller and Stavrakou, 2005; Delon et al., 2008; van der A et al., 2008). In comparison to most of the top-down studies, SNO_x seems to mostly be underestimated by the algorithm of Yienger and Levy (1995). Since the publication of YL95o many more measurements have been carried out and published than were available at the time of YL95o, which potentially reduce the discrepancy.

Here we present major improvements to the algorithm by YL95o and derive updated emission factors, calibrated in a bottom-up approach with a global dataset of measurements of SNO_x. We then compare our simulated emissions to the a posteriori top-down

ACPD
10, 16007–16054, 2010

emissions of Jaeglé et al. (2005).

2 Model framework and measurement dataset

For this study we applied the ECHAM/MESSy Atmospheric Chemistry (EMAC) model (ECHAM5 version 5.3.01, MESSy version 1.6), which is a numerical chemistry and climate simulation system that includes sub-models describing tropospheric and middle atmospheric processes and their interaction with oceans, land and human influences (Jöckel et al., 2006). It uses the first version of the Modular Earth Submodel System (MESSy1) to link multi-institutional computer codes. The core atmospheric model is the 5th generation European Centre Hamburg general circulation model ECHAM5 (Roeckner et al., 2006). The submodels switched on here were CLOUD, CONVECT (Tost et al., 2006), ONLEM (Kerkweg et al., 2006) and RAD4ALL.

We performed a simulation covering the period from 1990 to 2000 nudged by the ECMWF ERA40 data (Uppala et al., 2005), with a spherical truncation of T106 (approx. 1.1 by 1.1 degrees) and 31 pressure levels. SNO_x is calculated in the submodel ONLEM according to the algorithm by Yienger and Levy (1995) implemented by Ganzeveld et al. (2006) (hereafter called YL95e, "e" for EMAC).

From the above simulation we use the soil temperature and soil wetness as input parameters for an offline calculation of SNO_x, with improvements applied in 4 steps (each building on the previous step):

1. Introduction of a new landcover map, source of fertilizer data and new pulsing routine (LC)
2. Reduction of NO emission from fertilizer application (LC+FIE)
3. Using volumetric soil moisture instead of water column (LC+FIE+VSM)
4. Recalibration of emission factors with measurements (YL95/SL10)

ACPD
10, 16007–16054, 2010

2.1 State of the art model

The parameterization by YL95o distinguishes between two soil moisture states and calculates the emissions based on a statistically derived dry (A_d) and wet (A_w) emission factor for 12 different ecosystems and a temperature dependence according to the Eqs. (1a) and (1b) with T in °C.

$$F_{soil}(T, A_w) = \begin{cases} 0.28 \cdot T \cdot A_w & 0°C < T \leq 10°C \\ e^{0.103 \cdot T} \cdot A_w & 10°C < T \leq 30°C \\ 21.97 \cdot A_w & T > 30°C \end{cases} \quad (1a)$$

$$F_{soil}(T, A_d) = \begin{cases} \frac{T}{30} \cdot A_d & 0°C < T \leq 30°C \\ A_d & T > 30°C \end{cases} \quad (1b)$$

For rainforests, constant emissions were assumed for the dry and wet seasons. Agricultural areas are calculated like the wet grassland plus a fraction of the applied fertilizer (see further down). In the YL95e simulation the twelve ecosystems (Table 1, 4th column) defined by YL95o are based on the 72 ecosystems of Olson (1992).

The calculated flux is then multiplied by a pulsing factor which emulates the physical sudden pulse of NO, which is known to occur when precipitation falls after a dry period. If there has been no precipitation in a gridcell during the last 14 days, and the precipitation then exceeds 1 mm ("sprinkle"), 5 mm ("shower") or 15 mm ("heavy rain") during one day an increase of the emission rate by the factor in Eq. (2) is assumed, lasting for d days (the value on the far right is the pulse-inducing 24-h rain rate, for "sprinkle", "shower" and "heavy rain").

$$\text{pulse} = \begin{cases} 11.19 \cdot e^{-0.805 \cdot d} & 1 < d < 3; & 1-5 \text{mm/d} \\ 14.68 \cdot e^{-0.384 \cdot d} & 1 < d < 7; & 5-15 \text{mm/d} \\ 18.46 \cdot e^{-0.208 \cdot d} & 1 < d < 14; & >15 \text{mm/d} \end{cases} \quad (2)$$

ACPD
10, 16007–16054, 2010

If the pulsing criterion is not fulfilled, then pulse is set to 1. Thus the direct SNO_x from the soil into the vegetation layer is calculated as product of Eqs. (1ab) and (2):

$$SNO_x = \text{pulse} \cdot F_{\text{soil}}(T, A_{\text{w/d}}, [\text{fertilizer}]) \quad (3)$$

For the comparison with Jaeglé et al. (2005) SNO_x is finally partly removed via dry deposition in the vegetation layer, before it is released into the free troposphere, which is represented by the canopy reduction factor (CRF), calculated as:

$$CRF = \frac{e^{-k_s \cdot SAI} + e^{-k_c \cdot LAI}}{2} \quad (4)$$

with k_s and k_c representing stomata and cuticle absorptivity constants. SAI is the stomatal area index (ratio of stomatal area to leaf surface area) and LAI is the leaf area index (ratio of leaf surface to the geographical surface area). The calculation of CRF is originally based on a study by Jacob and Bakwin (1991), and is based on ecosystem and season specific stomatal area indices as well as a monthly leaf area index map. SNO_x^* effectively released to the atmosphere is thus calculated by multiplying Eq. (3) with Eq. (4):

$$SNO_x^* = CRF \cdot SNO_x \quad (5)$$

The SNO_x in the YL95e simulation without applying the CRF is depicted in Fig. 1.

2.2 Database of measurements

Yienger and Levy (1995) had far fewer measurements available when they developed their algorithm 15 years ago than there are today. They used data from 4 publications at 12 different sites to calculate the exponential factor for the wet emission between 10 and 30 °C (see Eq. 1a), and measurements from 24 sites in 6 of their ecosystems taken from 15 publications (plus two unpublished sites) were used to calculate the other emission factors under wet conditions. For the dry emission factor they used 9 sites (2 unpublished) in one ecosystem (grassland) taken from 7 publications. For one

ACPD
10, 16007–16054, 2010

ecosystem (dry deciduous forest), they did not indicate where the data comes from and for the others the dry emission factor is calculated as one third of the wet emission flux above 30 °C (see Eq. 1a), which gives $A_d = \frac{21.97}{3} A_w \approx 7.3 \cdot A_w$.

We have compiled, building on Stehfest and Bouwman (2006), a dataset consisting of 108 articles with 560 field measurements of SNO_x covering the period from 1976 to 2009, with 360 measurements during the simulation period. There are clear gaps in the measurements, e.g. in Central and Eastern Russia as well as between Saudi Arabia and India, which can be seen by the distribution of the measurement locations in Fig. 1.

We employ a more recent landcover system, based on the MODIS satellite data (Friedl et al., 2006) and combine this for some landcover classes with the Koeppen main climate classes (Kottek et al., 2006) (see Table 1), which doubles the number of landcover classes compared to YL95o. In order to reproduce the YL95o ecosystems, we associated the most similar ecosystem used in YL95o with the landcover class after Friedl et al. (2006) for each individual measurement based on the given description. For a better comparison to the tables, we call landcovers in A, B (and C) climates "warm", landcovers in (C), D and E climates "cold", and give the ID used in the tables in brackets. The database and additional information like soil properties and the literature references are made available in the electronic supplement.

The range of measured SNO_x spans from -6.89–$547\,ng\,m^{-2}\,s^{-1}$ in the whole dataset with a nearly log-normal distribution (Fig. 2), which is quite common for natural processes. There are the 19 measured fluxes less than $0\,ng\,m^{-2}\,s^{-1}$ and 8 measured fluxes equal to 0. We set these to $10^{-4}\,ng\,m^{-2}\,s^{-1}$, so that on the histogram a second small peak at -9.2 ($=-4 \cdot \ln(10)$) appears. We write the log-normal means and standard deviations as normal numbers (rather than in the exponential form, e.g., $e^{1.3\pm1.1}$ becomes $3.67^{+7.35}_{-2.45}$). By classifying the dataset by the MODIS landcover and additionally for some land cover classes of the Koeppen main climate, there are measurements in 13 of the 24 new landcover classes (Table 1), which are used later on. As can be seen in Fig. 3 the log-normal distribution again matches the distribution of the mea-

ACPD
10, 16007–16054, 2010

surements, when we ignore fluxes ≤0. In cold open shrubland (8) there was only one measurement, therefore no histogram can be shown.

Due to the large variations in the measured SNO_x fluxes and the coarse spatial model resolution in AC-GCMs we will use the full dataset for optimizing the calculation of SNO_x fluxes, rather than only the measured fluxes that were carried out during our simulation period (underlying this is an assumption of a relatively stable climate with annually varying weather and soil conditions during the measurement period). The database contains 203 measurements in agriculture, 219 measurements under more or less "undisturbed" or "natural" conditions and 138 measurements for anthropogenically altered conditions in the non-agricultural land covers. Anthropogenically altered conditions include fertilizer application, irrigation, liming, clearcutting and so on. Although the measurements under anthropogenic influence without agriculture ($4.29^{+16.08}_{-3.38}$) are, according to the Kolmogorov-Smirnov test with $p<10^{-3}$, significantly higher than under unperturbed natural conditions ($1.57^{+8.73}_{-1.33}$), we use all measurements in our analysis, and note that this may lead us to overestimate the emission factors. However, if we had used only the measurements under unperturbed natural conditions, we would not have had enough measurements in our new landcover classes for a satisfactory tuning of the emission factors.

3 Methods to improve the emission model

In Fig. 4 we compare the simulated flux of YL95e with the measured fluxes in our database for each ecosystem and Table 2 gives the mean values of the ecosystems. From this it is obvious that the flux from all the ecosystems (except tundra and rainforest) as well as the global simulated flux is underestimated by the algorithm, and an improvement is necessary.

We will now introduce the improvements which we implemented in the calculation of the SNO_x flux in our model and discuss the changes which were caused by these improvements. We discuss the change in the pulsing routine first, since this effects

ACPD
10, 16007–16054, 2010

all our new simulations beyond YL95e. The change in the underlying landcover map and the change in how fertilizer application is dealt with cannot be treated separately and are discussed in one step (LC). The LC case is also considered for the effects of resolution, before going on to the other individual developments.

3.1 Pulsing

In the YL95e algorithm as implemented previously in EMAC the amount of precipitation to initiate the pulsing was checked every time step; therefore the pulsing hardly ever reached its maximum range of values, and contributes only 3% to the total SNO_x in the YL95e simulation. From the LC simulation onwards, we check the precipitation of the last 24 h only once a day at 00:00 UTC, and the fraction attributed to pulsing increases to 17% (Table 3). Our new result is in the range of the 10–22% proposed by Davidson (1992) and it is much closer to the 24% originally simulated by YL95o, compared to the previous EMAC setup.

Nevertheless, we note that this is a simple implementation. In the literature some measurements show small pulses (Garcia-Montiel et al., 2003), while others show much larger pulses (Davidson et al., 1991). Too much rain could also reduce the diffusity of the soil (Rondón et al., 1993), which would reduce the strength of the pulse with strong precipitation events. Finally other events also generating pulses, like fire or plowing (Sanhueza, 1997) are not yet considered in our model.

3.2 Ecosystem/land cover (LC)

Instead of using the twelve ecosystems originally introduced by YL95o we use the 18 MODIS land cover classes (Friedl et al., 2006) for the year 2000 and merge them with the main climates of the Koeppen climate classification (Kottek et al., 2006) to yield a new total of 24 landcover types (Table 1).

The overall change in SNO_x from $9.24 \pm 0.16\,Tg(N)\,y^{-1}$ to $9.71 \pm 0.22\,Tg(N)\,y^{-1}$ due to the new landcover is very small even if we separately consider "natural" ecosystems

ACPD
10, 16007–16054, 2010

(0–20 in Table 1), changing from 5.21 Tg(N) y^{-1} to 5.91 Tg(N) y^{-1} and "anthropogenic" ecosystems (21–23) from 4.02 to 3.79 Tg(N) y^{-1}. Concerning the geographical distribution of anually simulated SNO_x, this step leads to:

- Increased emissions over Europe and Central USA (Fig. 5), especially due to the treatment of fertilizer (see next paragraph).
- Reduction in the emissions in Southern and Eastern Asia, because we reintroduced the reduction of SNO_x in the "rice-producing areas" as described in the original publication by YL95o, but which was not in YL95e as previously implemented in EMAC. This can be clearly seen by the unrealistic sharp and straight emission decrease in Eastern India and south of Bejing (see Sect. 5 for discussion).
- Lower emissions over large parts of Australia, the Southern Saudi Arabian peninsula and Somalia, which was prescribed as grassland in YL95e, while these regions are now dominated by shrublands.

3.3 Influence of model resolution

The focus of our simulations was on a fine resolution and we omitted the computationally expensive chemical processes in the atmosphere. When they are included, the model is usually run at a lower horizontal resolution. To investigate the influence of the resolution on SNO_x we performed three additional simulations at T21 (~5.6×5.6°), T42 (~2.8×2.8°) and T63 (~1.9×1.9°). The effect of the resolution is depicted in Fig. 6. SNO_x induced by precipitation (pulsing) for YL95e stays at a very low level, between 2 and 3% for all resolutions. We have two opposing effects here. First, with coarser horizontal resolution the model internal timestep increases to 20 min for T63, 30 min for T42 and 40 min for T21. The longer timesteps lead to more accumulated precipitation in one timestep. Second, with coaser horizontal resolution the convective precipitation is dispersed over a larger area, which leads to weaker pulses and less

ACPD
10, 16007–16054, 2010

likelihood of reaching the pulsing threshold. From the LC simulation onwards the first point (timestep dependence) does not contribute because the accumulated precipitation is checked only once a day, which leads to stonger and more frequent pulses with increasing resolution.

The general increase of the emission from both routines with finer resolution is due to the exponential dependence on the temperature in the calculation of the wet emission flux. Although the temperature of one gridbox in the lower resolution simulation will roughly equal the mean temperature of the corresponding set of gridboxes in the high resolution simulation, the peak temperatures will be greater at higher resolution, so that SNO_x will also be higher in the finer resolution simulation. One possibility to reduce the understimation in the coarser resolution simulations is to scale the emission factors or rather the emission flux by the ratio of the coarse resolution to the T106 resolution emission magnitude. Scaling the emission factors results in a notable improvement (Table 4) but still results in an underestimation, since the area of soils defined as wet increases slightly with increasing resolution and other unresolved unlinearities influence the simulation. Scaling the emission flux leads to an even larger overestimation, since the emission flux increases with decreasing latitude and the gridcell size increases, respectively, which results in a larger global simulated yearly emission.

3.4 Fertilizer induced NO emission (LC+FIE)

In YL95e the ecosystem map was overlaid with the cultivation index by Bouwman and Boumans (2002) and uses the same amount of applied fertilizer for each year, from which a certain fraction (0.7%) is emitted as FIE during the growing season. However, since agriculture is already defined in the ecosystem dataset, and is ignored as a separate ecosystem in YL95e, effectively some fraction of the emitting gridbox is neglected and SNO_x from model gridboxes with a fraction of agriculture is underestimated. This can also be seen if one sums up the ecosystem areas used for the calculation of the emission flux (values in brackets of column "YL95e" in Table 1), which gives a total world surface area of 5.04×10^8 km^2, less than the actual surface area of

ACPD
10, 16007–16054, 2010

of 5.1×10^8 km^2.

Here we use yearly varying fertilizer application based on the country based FAO fertilizer consumption rate provided by the United Nations Environment Programme (http://geodata.grid.unep.ch) and assume that the fertilizer is applied on the area of the last three landcover classes in Table 1. Since using this method results in unrealistic amounts of fertilizer usage for the Lesser Antilles and the islands east of Madagascar (up to 34 790 kg(N) ha^{-1} y^{-1}), we assumed an upper limit of 500 kg(N) ha^{-1} y^{-1}, which is high but should be viable, given that fertilizer applications up to 378–524 kg(N) ha^{-1} y^{-1} have been reported (Richter and Roelcke, 2000). This approach is still not very accurate, since for example fertilizer is not spatially and temporally distributed evenly over large countries like China (Ju et al., 2004). On the other hand since we use yearly varying fertilizer application rates, this already represents an improvement.

Yienger and Levy (1995) originally assumed a fraction of 2.5% of the applied fertilizer to be lost as NO. In our the dataset of measurements, the average amount of applied fertilizer is 137±74 kg(N) ha^{-1} y^{-1} and it was observed that the fraction emitted as NO was 1.0±2.1%. Based on this we set the FIE to 1% in our optimized simulation, which gives a global emission of 0.98 Tg(N) y^{-1} induced by fertilizer application, instead of 2.45 with an FIE of 2.5%. Thus we have reduced the global NO emissions by 1.47 Tg(N) y^{-1} by reducing the FIE in our simulation from 2.5% to 1%. The reduction is mainly located over the Central USA, Europe and Northeast Asia (Fig. 7).

Our calculated reduction of fertilizer fraction emitted as SNO_x is higher than the value of 0.55% calculated by Stehfest and Bouwman (2006) and the previous value by Bouwman and Boumans (2002) of 0.7%. Also the total yearly SNO_x from agriculture of 2.33 Tg(N) is higher than their estimate of 1.8 and 1.7 Tg(N), respectively, although our value is within the large range of uncertainty given by Stehfest and Bouwman (2006) (−80% and +406% for the 95% confidence interval).

Finally the reduction of SNO_x in the "rice-producing areas" is debatable (see Sect. 5). If we did not reduce the emissions there, we would increase the total emissions by

ACPD
10, 16007–16054, 2010

0.81 Tg(N) y^{-1}.

3.5 Soil moisture state (LC+FIE+VSM)

Yienger and Levy (1995) used the precipitation history to distinguish between the dry and wet soil conditions. In YL95e the water column in the soil was used instead. Since the simulation of soil moisture has improved substantially over the last decade, we can now make use of the volumetric soil moisture content, which can be calculated with the help of the root depth. We set the threshold for dry vs. wet conditions to 15% volumetric soil moisture content, which is for an average soil between the field capacity (amount of water that can be held by the soil against the gravitational force) and the permanent wilting point (at which plants can not take up the water anymore).

This has a major impact on the classes warm savannah (11), warm grassland (12) and woody savannah (13) with a decrease of yearly SNO_x flux by 0.41, 0.42, 0.11 Tg(N), respectively. Since these land cover classes are mostly present in the Sahel region, Eastern Africa and the Southern USA/Northern Mexico the emission from those regions are affected most (Fig. 8). In the other landcover classes the emissions are reduced by less than 0.01 Tg(N) y^{-1}, including cropland classes, which do not include an explicit dependence on the soil moisture, since it is assumed that due to irrigation the soil moisture is relatively constant and normally in the wet regime, although this assumption could possibly be improved in future studies. Thus the global yearly flux in the LC+FIE+VSM simulation is 7.28 Tg(N) y^{-1}.

3.6 Emission factors (YL95/SL10)

For each individual measurement we calculated the emission factor for the appropriate period of the whole simulation (individually for each year of the simulation, then determining the mean emission factor from this) as described below. In order to reduce the statistical error we used simulated monthly mean values for the whole months and not only for those days of a month for which measurements were available.

ACPD
10, 16007–16054, 2010

Since we have only the total SNO_x for each measurement and do not have time series of the measurements, accompanied with time series of temperature and soil moisture it is impossible to calculate the emission factors analytically. Therefore, to determine new emission factors for each measurement we iteratively computed the new emission factor, starting with the original emission factor by YL95o, then decreasing the difference between model and measurement by multiplication with a factor s or its reciprocal value (Eq. 6a,b) using Δf = measured flux − simulated flux and i is the number of the iteration step.

$$s = 1 + \frac{|\Delta f|^{0.8}}{50 + 50 * A_w} \tag{6a}$$

$$A_{w/d,i} = \begin{cases} s \cdot A_{w/d,i-1} & \text{for } \Delta f \geq 0 \\ \frac{1}{s} \cdot A_{w/d,i-1} & \text{for } \Delta f < 0 \end{cases} \tag{6b}$$

Since the measured range of NO fluxes spans over a few orders of magnitude (0.00289 to 547 $ng\,m^{-2}\,s^{-1}$), we set the convergence criterion to $\frac{\Delta f}{\text{measured flux}} \leq 10^{-4}$, after which we stopped the iteration. For measured negative fluxes (deposition) or zero flux we did not consider the measurement for our calculation of the new emission factors. Ignoring measurements less than or equal to zero (blue dashed line in Figs. 2 and 3) matches the distribution of measurements (black solid line) better than replacing them with by 10^{-4} (red dashed line). Due to the lack of time series data of the measured SNO_x we can not calculate the wet and dry emission factors separately and therfore we keep the ratio between the dry and wet factor constant at 7.3, like in the algorithm by YL95o. On average we reached $\frac{\Delta f}{\text{measured flux}} \leq 10^{-4}$ in 302 iteration steps with a maximum of 38 088 and a median of 86.

We calculated the new emission factors for each landcover class ($A_{w/d}$) according to Eq. (7), because the distribution of all measurements is, as already mentioned, approximately log-normal. We also weight each calculated emission factor by the length

ACPD
10, 16007–16054, 2010

of the measurement in d days.

$$A_{\mathrm{w/d}} = e^{\frac{\sum_{i=1}^{N}(\log(A_{\mathrm{w/d},i})\cdot d_i)}{\sum_{i=1}^{N} d_i}} \quad (7)$$

with $A_{\mathrm{w/d},i}$ beeing the wet and dry emission factors for each measurement i, and N measurements per land cover.

3.6.1 Results for iteration by region

As depicted in Fig. 1 we defined 5 regions with clusters of measurements. We abbreviate the regions as follows: EUR – Europe, NAM – North America, SAM – Central/South America + Hawaii, ASA – Asia and Australia and AFR – Africa. Here we recompute the emission factors individually for each region (Table 7). We discuss several of the key differences between the regions for selected land covers (for which there are measurements in multiple land covers), along with reasons for differences, e.g. different measured fluxes (Table 5), simulated soil temperature and moisture as well as other unaccounted factors. The unaccounted factors include primarily the amount of available nitrogen and the organic material and its quality, since SNO_x is mainly produced in the uppermost centimeters of the soil, including the organic layer (Jambert et al., 1994; Papke and Papen, 1998; Bargsten et al., 2010).

Cold savannah (10): For EUR compared to NAM we calculate an emission factor that is more than twice as high (values in Table 7), although the emissions are very similar (Table 5). The calculations for EUR were taken from 2 publications and for NAM from 3 publications. The difference is due to the simulated soil temperature, which is around 15 °C for nearly all measurements, except for 3 measurements in EUR with measured 2.06, 1.67 and 6.82 ng m^{-2} s^{-1} at 1 °C and for one with a flux of 1.9 ng m^{-2} s^{-1} at 6 °C. Thus, similar fluxes were measured in the two regions, but the simulated soil temperature differs. To explain this, the modeled soil temperature in Europe would have to be 10° higher, which is unlikely; therefore other unaccounted factors must exist, which cause these differences.

ACPD
10, 16007–16054, 2010

Warm savannah (11): Although the measured flux in SAM is higher than in AFR, we calculate higher emission factors for AFR than for SAM. This can be explained by both the soil moisture and the temperature. In AFR we have more days with a volumetric soil moisture below 15%, whereas in SAM the wet flux dominates. The mean temperatures in SAM are 27.0–29.4 °C, just slightly below 30 °C, while in AFR they are clearly below 30 °C for most of the 17 measurements (2 at 9.9 °C, 3 at 13–14.9 °C and 6 at 22.3–24.3 °C). Therefore a higher emission factor is necessary in AFR than in SAM, which indicates that other controlling factors might be missing in the algoritm.

Warm grassland (12): The emission factors calculated for EUR and especially ASA are much higher than for the other three regions. In EUR the mean soil temperatures are all below 20 °C and for ASA below 15 °C. In AFR, which also has a relatively high flux, the wet soil regime is dominant, resulting in a lower emission factor. The measured flux in NAM is low compared to the other regions, yielding a lower emission factor. Due to these reasons higher emission factors are needed in EUR and ASA.

Woody savannah (13): The emission factors are calculated to be higher in SAM than in AFR; since soil temperature and moisture do not differ very much, this is simply due to higher emission fluxes measured in SAM than in AFR.

Deciduous broadleaved forest (16): The calculated emission factors are higher in NAM than in EUR, mainly because the measured fluxes in NAM are higher than in EUR, and in EUR there are more wet emission events than in NAM.

Evergreen broadleaved forest (20): Most of the measurements were performed in SAM, for which the calculated emission factor is nearly the same as in AFR, while a lower emission factor is calculated for ASA due to lower measured fluxes than in SAM and AFR.

Agriculture (21): The emission factor is only calculated for wet soil conditions as proposed by YL95o. NAM has a similar mean measured emission flux to ASA, but the temperature is on average higher, resulting in a higher emission factor for ASA. In AFR we also calculate a high emission factor, but only two measurements were performed in agricultural areas in Africa with a high emission flux.

ACPD
10, 16007–16054, 2010

3.6.2 Global results used in YL95/SL10

For the new emission factors which we calculated for use in our YL95/SL10 simulation, we used the values listed in Table 3. If there were no measurements in a landcover class (IDs: 7, 9, 15, 17, 22, 23), we used the emission factor of the most similar class (see Table 1; the horizontal lines represent the groupings of landcover classes). For example, for deciduous needleleaved forest (17), we choose the same emission factor as for deciduous broadleaved forest in cold climate (16), since they are more similar than compared to evergreen needleleaved forests (Vogt et al., 1986).

In the step from LC+FIE+VSM to YL95/SL10 we find an increase of all emission factors in all landcover classes except for cold open shrubland (8) and mixed forests (14), which have globally insignificant differences, and warm savannah (11) and evergreen broadleaved forest in warm climates (20), where the emissions decrease by $0.41\,\mathrm{Tg(N)\,y^{-1}}$ (33%) and $1.74\,\mathrm{Tg(N)\,y^{-1}}$ (75%), respectively. In warm grassland (12), the previous reduction from LC+FIE to LC+FIE+VSM is not compensated by the increased emission factors here. On a global scale the decrease is only visible for the tropical regions (Fig. 9), where the latter two landcovers are mainly located.

The strongest increases (greater than $0.5\,\mathrm{Tg(N)\,y^{-1}}$) in the yearly global flux were simulated for woody savannah (13), deciduous needleleaved forest (17) and cropland (21) with 1.34 (265%), 0.67 (4397%) and $0.45\,\mathrm{Tg(N)\,y^{-1}}$ (26%) increases, respectively. In all this leads to an increase of $1.74\,\mathrm{Tg(N)\,y^{-1}}$ (24%) compared to the LC+FIE+VSM simulation.

Since we increase the emission from agricultural areas (21–23) to $2.93\,\mathrm{Tg(N)}$ we further depart from the values of Stehfest and Bouwman (2006) and Bouwman and Boumans (2002) compared to the LC+FIE simulation, but are still within their 95% confidence interval. The new total $\mathrm{SNO_x}$ flux is now $9.01\,\mathrm{Tg(N)\,y^{-1}}$. If we were to leave out the reduction in the "rice-producing areas", we would get an additional increase of $1.04\,\mathrm{Tg(N)\,y^{-1}}$.

ACPD
10, 16007–16054, 2010

3.7 Canopy reduction factor (CRF)

We also use an updated map of the leaf area index (LAI), published by Deng et al. (2006), to calculate the canopy reduction factor (CRF), which is relevant for the later comparision with Jaeglé et al. (2005).

The simulated reduction factor by the canopy layer varies on a monthly basis between 0.76 (northern hemispheric winter) and 0.88 (northern hemispheric summer) with a nearly constant interannual reduction of 0.81 in YL95/SL10, so that 7.49 Tg(N) y^{-1} enter the atmosphere from the canopy layer as SNO_x^* (see Sect. 2.1). In the YL95e simulation the reduction varies between 0.69 and 0.77 with an interannual mean of 0.72 and therefore a lower flux of 6.64 Tg(N) y^{-1} to the atmosphere. The weaker canopy reduction in YL95/SL10 is due to the higher agricultural emissions, where the reduction is lower (CRF+0.85) and due to the reduced emissions in evergreen deciduous forest (20) with a CRF of 0.54. Also the desert and shrub landcovers, which now have emissions and a very low CRF (0.88–0.99), contribute to a smaller reduction by the vegetation layer.

4 Comparison to satellite-derived emission estimates

Since we used all available measurements to provide the best statistics for tuning our emission factors, there are no independent in situ measurements left to evaluate our new implementation of the SNO_x algorithm by Yienger and Levy (1995). Therefore we compare our simulated above canopy flux with the a posteriori SNO_x fluxes of Jaeglé et al. (2005) for the year 2000 (Fig. 10), which are partly constrained by independent satellite-based measurements. In the total global flux our result (7.49 Tg(N) y^{-1}) differs by 15% from their yearly total flux of 8.84 Tg(N) y^{-1} and is closer to Jaeglé et al. (2005) than the 6.64 Tg(N) y^{-1} above canopy flux in YL95e and 5.5 Tg(N) y^{-1} in YL95o. Jaeglé et al. (2005) also use the algorithm by Yienger and Levy (1995) in their apriori simulations, but implemented in another global climate model. Therefore differences in the SNO_x flux can be due to a difference in the soil moisture states and in the temperature

ACPD
10, 16007–16054, 2010

values used in the calculations. But, what makes the largest difference between their results and ours might be the underlying landcover map, as we have already seen in the step from YL95e to LC. And another difference might result from their algorithm applied to the satellite and model data to distinguish between the NO sources (soil, fossil fuel burning, and biomass burning). Comparing Fig. 10a with Fig. 9a we see that many of the features of our simulated bottom-up distribution are similar to their top-down study, though there are notable differences, which are highlighted in Fig. 10b. There are several reasons for the simulated differences, as discussed below.

We calculate higher emissions in large areas of Europe except Spain, where Jaeglé et al. (2005) compute much higher emissions. Our simulated flux is also higher in other regions as can be seen in Fig. 10. However, in other regions our simulated flux is lower. Over the tropical rainforest, where SNO_x has the strongest impact on chemical processes in the atmosphere (Steinkamp et al., 2009) the emission is similar for our YL95/SL10 simulation and Jaeglé et al. (2005). It is worth noting that this reduction in the tropical emissions compared to YL95e (see Fig. 11 for difference between Jaeglé et al. (2005) and YL95e) will reduce the influence of SNO_x on global ozone chemistry, while on the other hand the general increase in SNO_x will in turn increase the influence.

The reduced flux over arid regions of the Middle East to Pakistan, the Sahel region and Australia may be explained by different landcover classes. Especially along the Northern African Mediterranean coast, agricultural areas in our land cover map seem to be much smaller compared to Pongratz et al. (2008). In the mountainous regions along the American west coast we also get lower emissions and we contend that it seems more sensible to have lower emissions from such regions of high altitudes. Furthermore, the higher emissions in our simulation from agriculture in the central and eastern parts of North America are reasonable compared to independent land usage distributions (Pongratz et al., 2008; Sterling and Ducharne, 2008). In the tropical region of South America our results agree well and are a clear improvement over YL95e. But over tropical Africa our simulated SNO_x is still lower than the results by Jaeglé et al. (2005).

ACPD
10, 16007–16054, 2010

5 Discussion

As expected, the mean value of the mesurements are in good agreement with the ones simulated with the tuned SNO_x fluxes in YL95/SL10 (Table 6 and Fig. 12). The small deviations occur, because we used exactly the corresponding start and end day of the measurements here, which gives a rough estimate of the statistical error. But we still have a very "cloudy" distribution around the 1:1 line (Fig. 12), which we expected for this kind of statistical model, since there are a lot of unaccounted parameters within each land cover class, like the heterogenity in soil parameters or the adaptation of NO producing microorganisms to different habitats. This is reflected in the logarithmic density distribution functions of the measurements (Fig. 13), which have much larger tails compared to the simulated fluxes.

A similar analysis like that performed in Sect. 3.6.1 can be performed by classifying the database by the duration of the measurements (Table 8). Even though there were only a few land cover classes (5, 11, 14, 19) with short term measurements (less than 3 months), one might expect that short term measurements will often have been performed to measure special events, like rain induced pulsing or fertilizer induced emission, so that the limitation to longterm measurements in our analyses would cause the calculated emission factor to decrease. However, we did not find this to be the case (see Table 8). No connection can be made between the length of the measurement and the calculation of the new emission factors.

The reduction of SNO_x in "rice-producing areas" was implemented by Yienger and Levy (1995) based on one publication. A more recent publication (FAO and IFA, 2001) stated that there are not enough measurements available to draw any conclusions on this. However, Zheng et al. (2003) reported that periodic flooding during rice production decreases the SNO_x even during non-flooded periods. Furthermore Fang and Mu (2009) found in a field campaign that the flux from rice fields is lower compared to other vegetable fields. Our simulation with the reduction in "rice-producing areas" agrees better with Jaeglé et al. (2005) than the old algorithm without the reduction in YL95e,

ACPD
10, 16007–16054, 2010

from which we conclude that keeping the original reduction of SNO_x in these regions is justified, until a better approach is found.

Although we doubled the number of landcover classes there are still large differences within individual classes, pointed out by comparing the continental/regional differences within one landcover class and the density distribution depicted in Fig. 13. The measured fluxes show a much more widely-stretched distribution compared to our simulated values within one landcover and the distribution of the measured values show a much stronger bi- to multimodal distribution. Other important limitations of our improved algorithm are:

- The gridbox size of more than 100×100 km is too large to accurately reproduce the measured fluxes; even if we were to decrease the cell size to a few orders of magnitude, this would not be sufficent to simulate the heterogenity.
- Instead of having only two soil moisture regimes, in reality one would expect a continous mathematical relationship such as that proposed and confirmed in laboratory measurements by Meixner and Yang (2006).
- Even if the algorithm was perfect, the use of simulated soil moisture and soil temperature could lead to unquantified errors, since they have not yet been evaluated for ECHAM5 or EMAC simulations.

Ideally the optimization we performed here must be repeated for each resolution at which the model is running, otherwise SNO_x will be underestimated at coarser resolutions and overestimated at finer resolutions (Fig. 6). We could improve the total yearly flux of the lower resolution by simply increasing the emission by the relative difference in the resolutions, but this would still be insufficent, due to non-linearities in the simulations. The areal fraction of soils defined as "wet" is slightly increasing with finer resolution which also increases SNO_x at higher temperatures.

ACPD
10, 16007–16054, 2010

6 Conclusions and outlook

We presented here a simple method to retune the soil NO emission algorithm according to Yienger and Levy (1995) using new measurements, along with several other improvements to the algorithm. Although the total global flux does not change dramatically, due to several opposing factors, we obtain a significant difference in the geographical distribution of SNO_x. The overall increase in SNO_x, contrasted with the reduction of SNO_x in tropical regions compared to the implementation by Ganzeveld et al. (2006) will in turn reduce the relative influence on the reaction chain from SNO_x through O_3 and OH to the oxidizing efficiency, as discussed in Steinkamp et al. (2009).

As long as there is no mechanistically based algorithm to calculate SNO_x, which might not be developed in the near future due to the heterogenity of soils, vegetation and microorganisms, a valuable approach is to continue tuning the calculation of SNO_x with available measurements. Since the algorithm by Yienger and Levy (1995) is the most-widely applied method to calculate SNO_x in AC-GCMs, the method we presented here can also be easily applied in other models. And with a growing amount of measurements of SNO_x accompanied with the measurement of other relevant factors, it should eventually be possible to draw more and more measurements closer to the 1:1 line by incorporating other factors in the parameterization.

Acknowledgements. We would like to thank Stefan Hagemann from the MPI for Meteorology in Hamburg for the calculation of the volumetric soil moisture, Jos Lelieveld for the initial idea and very fruitfull discussions, as well as Wolgang Wilcke for his constructive comments. Lyatt Jaeglé for providing her a posteriori top-down satellite data and the EMAC developers and users for their support, especially L. N. Ganzeveld, P. Jöckel, A. Kerkweg and H. Tost. Jörg Steinkamp apreciates the financial support by the International Max Planck Research School (IMPRS) for atmosperic chemistry and physics.

The service charges for this open access publication have been covered by the Max Planck Society.

ACPD

10, 16007–16054, 2010

References

Bargsten, A., Falge, E., Pritsch, K., E., Huwe, B., and Meixner, F. X.: Laboratory measurements of nitric oxide release from forest soil with a thick organic layer under different understory types, Biogeosciences, 7, 1425–1441, doi:10.5194/bg-7-1425-2010, 2010. 16021

Bertram, T. H., Heckel, A., Richter, A., Burrows, J. P., and Cohen, R. C.: Satellite measurements of daily variations in soil NO_x emissions, Geophys. Res. Lett., 32, L24812, doi:10.1029/2005GL024640, 2005. 16009

Bouwman, A. F. and Boumans, L. J. M.: Emissions of N_2O and NO from fertilized fields: summary of available measurement data, Global Biogeochem. Cy., 16, 1058, doi:10.1029/2001GB001811, 2002. 16017, 16018, 16023, 16034

Chameides, W. L., Fehsenfeld, F., Rodgers, M. O., Cardelino, C., Martinez, J., Parrish, D., Lonneman, W., Lawson, D. R., Rasmussen, R. A., Zimmermann, P., Greenberg, J., Middleton, P., and Wang, T.: Ozone precursor relationships in the ambient atmosphere, J. Geophys. Res., 97, 6037–6055, 1992. 16009

Davidson, E. A.: Pulses of nitric oxide and nitrous oxide flux following wetting of dry soil: an assessment of probable sources and importance relative to annual fluxes, Ecol. Bull., 42, 149–155, 1992. 16015

Davidson, E. A. and Kingerlee, W.: A global inventory of nitric oxide emissions from soils, Nutr. Cycl. Agroecosys., 48, 37–50, 1997. 16009

Davidson, E. A., Vitousek, P. M., Matson, P. A., Riley, R., García-Méndez, G., and Maass, J. M.: Soil emissions of nitric oxide in a seasonally dry tropical forest in México, J. Geophys. Res., 96, 15439–15445, 1991. 16015

Delon, C., Reeves, C. E., Stewart, D. J., Sera, D., Dupont, R., Mari, C., Chaboureau, J.-P., and Tulet, P.: Biogenic nitrogen oxide emissions from soils – impact on NO_x and ozone over West Africa during AMMA (African Monsoon Multidisciplinary Experiment): modelling study, Atmos. Chem. Phys., 8, 2351–2363, doi:10.5194/acp-8-2351-2008, 2008. 16009

Deng, F., Chen, J. M., Plummer, S., Chen, M., and Pisek, J.: Algorithm for global Leaf Area Index retrieval using satellite imagery, IEEE T. Geosci. Remote, 44, 2219–2229, 2006. 16024

Denman, K. L., Brasseur, G., Chidthaisong, A., Ciais, P., Cox, P. M., Dickinson, R. E., Hauglustaine, D., Heinze, C., Holland, E., Jacob, D., Lohmann, U., Ramachandran, S., da Silva Dias, P. L., Wofsy, S. C., and Zhang, X.: Couplings Between Changes in the Climate System and Biogeochemistry, in: Climate Change 2007: The Physical Science Basis. Contribution of

ACPD
10, 16007–16054, 2010

Working Group I to the Fourth Assessment Report of the Intergovernmental Panel on Climate Change, edited by: Solomon, S., Qin, D., Manning, M., Chen, Z., Marquis, M., Averyt, K. B., Tignor, M., and Miller, H. L., 499–587, Cambridge University Press, Cambridge, United Kingdom and New York, NY, USA, 2007. 16009

Fang, S. and Mu, Y.: NO_x fluxes from several typical agricultural fields during summer-autumn in the Yangtse Delta, China, Atmos. Environ., 43, 2665–2671, doi:10.1016/j.atmosenv.2009.02.027, 2009. 16026

FAO and IFA: Global estimates of gaseous emissions of NH_3, NO and N_2O from agricultural land, FAO and IFA, Rome, 2001. 16026

Friedl, M. A., McIver, D. K., Hodges, J. C. F., Zhang, X. Y., Muchoney, D., Strahler, A. H., Woodcock, C. E., Gopal, S., Schneider, A., Cooper, A., Baccini, A., Gao, F., and Schaaf, C.: Global land cover mapping from MODIS: algorithms and early results, Remote Sens. Environ., 83, 287–302, 2006. 16013, 16015

Ganzeveld, L. N., Lelieveld, J., Dentener, F. J., Krol, M. C., Bouwman, A. F., and Roelofs, G.-J.: Global soil-biogenic NO_x emissions and the role of canopy processes, J. Geophys. Res., 107, 4321, doi:10.1029/2001JD001289, 2002. 16009

Ganzeveld, L. N., van Aardenne, J. A., Butler, T. M., Lawrence, M. G., Metzger, S. M., Stier, P., Zimmermann, P., and Lelieveld, J.: Technical Note: Anthropogenic and natural offline emissions and the online EMissions and dry DEPosition submodel EMDEP of the Modular Earth Submodel system (MESSy), Atmos. Chem. Phys. Discuss., 6, 5457–5483, doi:10.5194/acpd-6-5457-2006, 2006. 16010, 16028

Garcia-Montiel, D. C., Steudler, P. A., Piccolo, M., Neill, C., Melillo, J., and Cerri, C. C.: Nitrogen oxide emissions following wetting of dry soils in forest and pastures in Rondônia, Brazil, Biogeochemistry, 64, 319–336, 2003. 16015

Hauglustaine, D. A., Hourdin, F., Jourdain, L., Filiberti, M.-A., Walters, S., Lamarque, J.-F., and Holland, E. A.: Interactive chemistry in the Laboratoire de Météorologie Dynamique general circulation model: description and background tropospheric chemistry evaluation, J. Geophys. Res., 109, D04341, doi:10.1029/2003JD003957, 2004. 16009

Horowitz, L. W., Walters, S., Mauzerall, D. L., Emmons, L. K., Rasch, P. J., Granier, C., Tie, X., Lamarque, J.-F., Schultz, M. G., Tyndall, G. S., Orlando, J. J., and Brasseur, G. P.: A global simulation of tropospheric ozone and related tracers: description and evaluation of MOZART, version 2, J. Geophys. Res., 108, 4784, doi:10.1029/2002JD002853, 2003. 16009

Jacob, D. J. and Bakwin, P. S.: Cycling of NO_x in tropical forest canopies, in: Microbial produc-

ACPD
10, 16007–16054, 2010

tion and consumption of greenhouse gases: methane, nitrogen oxides, and halomethanes, edited by: Rogers, J. E. and Whitman, W. B., pp. 237–254, American Society for Microbiology, Washington, D.C., USA, 1991. 16012

Jaeglé, L., Steinberger, L., Martin, R. V., and Chance, K.: Global partitioning of NO_x sources using satellite observations: relative roles of fossil fuel combustion, biomass burning and soil emissions, Faraday Discuss., 130, 407–423, 2005. 16009, 16010, 16012, 16024, 16025, 16026, 16051, 16052

Jambert, C., Delmas, R. A., Labroue, L., and Chassin, P.: Nitrogen compound emissions from fertilized soils in a maize field pine tree forest agrosystem in the southwest of France, J. Geophys. Res., 99, 16523–16530, 1994. 16021

Jöckel, P., Tost, H., Pozzer, A., Brühl, C., Buchholz, J., Ganzeveld, L., Hoor, P., Kerkweg, A., Lawrence, M. G., Sander, R., Steil, B., Stiller, G., Tanarhte, M., Taraborrelli, D., van Aardenne, J., and Lelieveld, J.: The atmospheric chemistry general circulation model ECHAM5/MESSy1: consistent simulation of ozone from the surface to the mesosphere, Atmos. Chem. Phys., 6, 5067–5104, doi:10.5194/acp-6-5067-2006, 2006. 16010

Ju, X., Liu, X., Zhang, F., and Roelcke, M.: Nitrogen fertilization, soil nitrate accumulation and policy recommendations in several agricultural regions of China, Ambio, 33, 300–305, 2004. 16018

Kampstra, P.: Beanplot: a boxplot altenative for visual comparison of distributions, J. Stat. Softw., 28, 1–9, 2008. 16054

Kerkweg, A., Sander, R., Tost, H., and Jöckel, P.: Technical note: Implementation of prescribed (OFFLEM), calculated (ONLEM), and pseudo-emissions (TNUDGE) of chemical species in the Modular Earth Submodel System (MESSy), Atmos. Chem. Phys., 6, 3603–3609, doi:10.5194/acp-6-3603-2006, 2006. 16010

Kottek, M., Grieser, J., Beck, C., Rudolf, B., and Rubel, F.: World map of the Köppen-Geiger climate classification updated, Meteorol. Z., 15, 259–263, 2006. 16013, 16015

Lawrence, M. G., Crutzen, P. J., Rasch, P. J., Eaton, B. E., and Mahowald, N. M.: A model for studies of tropospheric photochemistry: description, global distributions, and evaluation, J. Geophys. Res., 104, 26245–26277, 1999. 16009

Martin, R. V., Jacob, D. J., Chance, K., Kurosu, T. P., Palmer, P. I., and Evans, M. J.: Global inventory of nitrogen oxide emissions constrained by space-based observations of NO_2 columns, J. Geophys. Res., 108, 4537, doi:10.1029/2003JD003453, 2003. 16009

Martin, R. V., Sioris, C. E., Chance, K., Ryerson, T. B., Bertram, T. H., Wooldridge, P. J.,

ACPD

10, 16007–16054, 2010

Simulated biogenic soil NO emission improvement

J. Steinkamp and M. G. Lawrence

Cohen, R. C., Neuman, J. A., Swanson, A., and Flocke, F. M.: Evaluation of space-based constraints on global nitrogen oxide emissions with regional aircraft measurements over and downwind of Eastern North America, J. Geophys. Res., 111, D15308, doi:1.10.29/2005JD006680, 2006. 16009

Meixner, F. X. and Yang, W. X.: Biogenic emissions of nitric oxide and nitrous oxide from arid and semi-arid land, in: Dryland Ecohydrology, edited by: D'Odoricoand, P. and Porporat, A., 233–255, Springer, Dordrecht, The Netherlands, 2006. 16027

Müller, J.-F. and Stavrakou, T.: Inversion of CO and NO_x emissions using the adjoint of the IMAGES model, Atmos. Chem. Phys., 5, 1157–1186, doi:10.5194/acp-5-1157-2005, 2005. 16009

Olson, J.: World ecosystems (WE1.4): Digital raster data on a 10 min geographic 1080×2160 grid square, in: Global ecosystems database, Version 1.0: DISC A, edited by: Kineman, J. and Ochrenschall, M., NOAA National Geophysical Data Center, Boulder, Colorado, USA, 1992. 16011, 16034

Papke, H. and Papen, H.: Influence of acid rain and liming on fluxes of NO and NO_2 from forest soil, Plant Soil, 199, 131–139, 1998. 16021

Pongratz, J., Reick, C., Raddatz, T., and Claussen, M.: A reconstruction of global agricultural areas and land cover for the last millennium, Global Biogeochem. Cy., 22, GB3018, doi:10.1029/2007GB003153, 2008. 16025

Richter, J. and Roelcke, M.: The N-cycle as determined by intensive agriculture – examples from central Europe and China, Nutr. Cycl. Agroecosys., 57, 33–46, 2000. 16018

Roeckner, E., Brokopf, R., Esch, M., Giorgetta, M., Hagemann, S., Kornblueh, L., Manzini, E., Schlese, U., and Schulzweida, U.: Sensitivity of simulated climate to horizontal and vertical resolution in the ECHAM5 atmosphere model, J. Climate, 19, 3771–3791, 2006. 16010

Rondón, A., Johansson, C., and Sanhueza, E.: Emission of nitric oxide from soils and termite nests in a trachypogon savanna of the Orinoco Basin, J. Atmos. Chem., 17, 293–306, 1993. 16015

Sanhueza, E.: Impact of human activity on NO soil fluxes, Nutr. Cycl. Agroecosys., 48, 61–68, 1997. 16015

Stehfest, E. and Bouwman, L.: N_2O and NO emission from agricultural fields and soils under natural vegetation: summarizing available measurement data and modeling of global annual emissions, Nutr. Cycl. Agroecosys., 24, 207–228, 2006. 16013, 16018, 16023

Steinkamp, J., Ganzeveld, L. N., Wilcke, W., and Lawrence, M. G.: Influence of modelled soil

ACPD
10, 16007–16054, 2010

biogenic NO emissions on related trace gases and the atmospheric oxidizing efficiency, Atmos. Chem. Phys., 9, 2663–2677, doi:10.5194/acp-9-2663-2009, 2009. 16009, 16025, 16028

Sterling, S. and Ducharne, A.: Comprehensive data set of global land cover change for land surface model applications, Global Biogeochem. Cy., 22, GB3017, doi:10.1029/2007GB002959, 2008. 16025

Tost, H., Jöckel, P., and Lelieveld, J.: Influence of different convection parameterisations in a GCM, Atmos. Chem. Phys., 6, 5475–5493, doi:10.5194/acp-6-5475-2006, 2006. 16010

Uppala, S. M., Kallberg, P. W., Simmons, A. J., Andrae, U., Bechtold, V. D., Fiorino, M., Gibson, J. K., Haseler, J., Hernandez, A., Kelly, G. A., Li, X., Onogi, K., Saarinen, S., Sokka, N., Allan, R. P., Andersson, E., Arpe, K., Balmaseda, M. A., Beljaars, A. C. M., Van De Berg, L., Bidlot, J., Bormann, N., Caires, S., Chevallier, F., Dethof, A., Dragosavac, M., Fisher, M., Fuentes, M., Hagemann, S., Holm, E., Hoskins, B. J., Isaksen, L., Janssen, P. A. E. M., Jenne, R., McNally, A. P., Mahfouf, J. F., Morcrette, J. J., Rayner, N. A., Saunders, R. W., Simon, P., Sterl, A., Trenberth, K. E., Untch, A., Vasiljevic, D., Viterbo, P., and Woollen, J.: The ERA-40 re-analysis, Q. J. Roy. Meteor. Soc., 131, 2961–3012, doi:10.1256/qj.04.176, 2005. 16010

van der A, R. J., Eskes, H. J., Boersma, K. F., van Noije, T. P. C., Van Roozendael, M., De Smedt, I., Peters, D. H. M. U., and Meijer, E. W.: Trends, seasonal variability and dominant NO_x sources derived from a ten year record of NO_2 measured from space, J. Geophys. Res., 113, D04302, doi:10.1029/2007JD009021, 2008. 16009

Vogt, K. A., Grier, C. C., and Vogt, D. J.: Production, turnover, and nutrient dynamics of above- and belowground detritus of world forests, Adv. Ecol. Res., 15, 303–377, 1986. 16023

Yienger, J. J. and Levy, H.: Empirical model of global soil-biogenic NO_x emissions, J. Geophys. Res., 100, 11447–11464, 1995. 16008, 16009, 16010, 16012, 16018, 16019, 16024, 16026, 16028, 16036, 16040, 16041

Zheng, X., Huang, Y., Wang, Y., and Wang, M.: Seasonal characteristics of nitric oxide emission from a typical Chinese rice-wheat rotation during the nonwaterlogged period, Global Change Biol., 9, 219–227, 2003. 16026

ACPD

10, 16007–16054, 2010

Table 1. World surface areas of the YL95e ecosystems and new YL95/SL10 land cover classes in the EMAC model. For YL95e the first number is as adopted from Olson (1992) and the number in brackets gives the area reduced by (1 – cultivation index) for non-agricultural areas and the cultivated area for agriculture with the cultivation index after Bouwman and Boumans (2002).

ID	MODIS landcover	Köppen main climate[a]	YL95e ecosystem	Area [10^6 km^2] YL95/SL10	YL95e
0	Water	—	Water	364.18	367.15 (364.3)
1	Permanent wetland	—		0.30	
2	Snow and ice	—	Ice	16.12	15.44 (15.44)
3	Barren	D, E		2.28	
4	Unclassified	—		0.07	
5	Barren	A, B, C	Desert	17.68	17.23 (16.71)
6	Closed shrubland	—	Shrubland	0.75	0 (0)
7	Open shrubland	A, B, C		14.85	
8	Open shrubland	D, E	Tundra	11.85	11.61 (11.36)
9	Grassland	D, E		0.46	
10	Savannah	D, E		4.66	
11	Savannah	A, B, C	Grassland	9.76	33.10 (27.12)
12	Grassland	A, B, C		8.80	
13	Woody savannah	—	Woodland	10.94	14.16 (7.98)
14	Mixed forest	—	Dec. forest	6.87	5.07 (3.41)
15	Evergr. broadl. forest	C, D, E		1.97	
16	Dec. broadl. forest	C, D, E		1.66	
17	Dec. needlel. forest	—		0.93	
18	Evergr. needlel. forest	—	Conif. forest	5.78	15.81 (14.45)
19	Dec. broadl. forest	A, B	Dry dec. forest	0.62	4.70 (3.68)
20	Evergr. broadl. forest	A, B	Rainforest	12.76	10.40 (9.12)
21	Cropland	—	Agriculture	13.13	15.48 (30.01)
22	Urban and build-up lands	—		0.73	
23	Cropland/nat. veg. mosaic	—		3.01	

[a] A: equatorial, B: arid, C: warm temperate, D: snow, E: polar

ACPD
10, 16007–16054, 2010

Table 2. Measured and simulated SNO_x for the YL95e ecosystems (in $ng\,m^{-2}\,s^{-1}$). Measurements are taken from our database (numbers per ecosystem in brackets) and the simulated SNO_x values are for the corresponding period of each calculated year.

Ecosystem	*N*	measured	YL95e
Tundra	11 (1)	0.03^{+0}_{-0}	$0.22^{+0}_{-0.03}$
Grassland	1675 (154)	$3.94^{+21.22}_{-3.32}$	$2.27^{+12.21}_{-1.11}$
Woodland	44 (4)	$7.24^{+105.64}_{-6.78}$	$2.63^{+38.33}_{-0.54}$
Deciduous forest	227 (22)	$1.11^{+3.29}_{-0.83}$	$0.08^{+0.24}_{-0.05}$
Coniferous forest	706 (66)	$4.28^{+17.15}_{-3.42}$	$0.08^{+0.33}_{-0.06}$
Drought deciduous forest	117 (11)	$5.37^{+13.01}_{-3.8}$	$0.36^{+0.88}_{-0.12}$
Rainforest	552 (51)	$1.51^{+5.75}_{-1.2}$	$5.36^{+20.39}_{-1.59}$
Agriculture	2000 (185)	$5.12^{+29.69}_{-4.37}$	$3.23^{+18.74}_{-2.07}$
All ecosystems	5332 (494)	$3.29^{+17.44}_{-2.76}$	$1.41^{+7.51}_{-1.19}$

ACPD
10, 16007–16054, 2010

Table 3. The original (YL95e) and adopted (YL95/SL10) emission factors of the soil biogenic NO emission algorithm based on the Yienger and Levy (1995) algorithm. When not shown, standard deviations are less than or equal to 0.001.

	Emission factors[a]				Emission $\left[\frac{\text{Tg(N)}}{\text{year}}\right]$, pulsing fraction in brackets		
ID	YL95e		YL95/SL10		YL95e	LC	YL95/SL10
0	0	0	0	0	0	0	0
1	0	0	0	0		0	0
2	0	0	0	0	0	0	0
3	0	0	0	0		0	0
4	0	0	0	0		0	0
5	0	0	$0.06^{+0.02}_{-0.02}$	$0.43^{+0.15}_{-0.11}$	0	0	0.2±0.01 (8%)
6	0	0	$0.09^{+0.31}_{-0.07}$	$0.65^{+2.24}_{-0.50}$	0	0	0.02 (19%)
7	0	0	$0.09^{+0.31}_{-0.07}$	$0.65^{+2.24}_{-0.50}$		0	0.33±0.01 (20%)
8	0.05	0.37	$0.01^{+0.00}_{-0.00}$	$0.05^{+0.01}_{-0.01}$	0.02 (3%)	0.03±0.002	0.01 (17%)
9	0.05	0.37	$0.84^{+1.43}_{-0.53}$	$6.17^{+10.42}_{-3.88}$		0.002	0.03 (17%)
10	0.05	0.37	$0.84^{+1.43}_{-0.53}$	$6.17^{+10.42}_{-3.88}$		0.03	0.34±0.01 (20%)
11	0.36	2.65	$0.24^{+1.71}_{-0.21}$	$1.76^{+12.56}_{-1.54}$	3.0±0.05 (2%)	1.65±0.03	0.82±0.01 (14%)
12	0.36	2.65	$0.42^{+2.02}_{-0.35}$	$3.06^{+14.73}_{-2.53}$		1.17±0.02	0.87±0.02 (19%)
13	0.17	1.44	$0.62^{+0.57}_{-0.30}$	$5.28^{+4.82}_{-2.52}$	0.45±0.01 (3%)	0.61±0.01	1.85±0.03 (14%)
14	0.03	0.22	$0.02^{+0.23}_{-0.01}$	$0.12^{+1.66}_{-0.11}$	0.02 (2%)	0.03	0.02±0.03 (15%)
15	0.03	0.22	$0.36^{+1.12}_{-0.27}$	$2.39^{+7.44}_{-1.81}$		0.02	0.17 (14%)
16	0.03	0.22	$0.36^{+1.12}_{-0.27}$	$2.39^{+7.44}_{-1.81}$		0.01	0.12 (16%)
17	0.03	0.22	$0.36^{+1.12}_{-0.27}$	$2.39^{+7.44}_{-1.81}$		0.002	0.02 (18%)
18	0.03	0.22	$1.35^{+6.38}_{-1.11}$	$9.88^{+46.66}_{-8.15}$	0.03 (3%)	0.02	0.68±0.03 (17%)
19	0.06	0.4	$0.08^{+0.14}_{-0.05}$	$0.62^{+1.03}_{-0.39}$	0.09 (3%)	0.02	0.02 (13%)
20	2.6	8.6	$0.44^{+2.27}_{-0.37}$	$2.47^{+11.17}_{-2.02}$	1.6±0.1 (3%)	2.33±0.05	0.58±0.01 (11%)
21	0.36		$0.52^{+2.29}_{-0.42}$		4.03±0.04 (3%)	2.78±0.17	2.16±0.1 (21%)
22	0.36		$0.52^{+2.29}_{-0.42}$			0.21±0.007	0.14 (18%)
23	0.36		$0.52^{+2.29}_{-0.42}$			0.81±0.03	0.62±0.02 (19%)
sum					9.24±0.16 (3%)	9.71±0.22	

[a] Wet/dry emission factors; values in brackets are the used emission factors.

ACPD
10, 16007–16054, 2010

Table 4. Relative yearly underestimation of SNO_x in the coarser simulations compared to the T106 resolution of the YL95e and LC simulation. Relative under- and overestimation if the emission factors or rather the gridcell emission flux is scaled by the previous underestimation. And the global area defined as wet in $10^6\,km^2$ (which equals $111.8\times10^6\,km^2$ for the T106 simulation).

	T21	T42	T63
YL95e	11.8%	4.3%	2.1%
	(4.6%, 9.6%)	(2.1%, 13.5%)	(1.8%, 13.2%)
LC	13.1%	7.2%	2.3%
	(5.6%, 10.1%)	(3.3%, 20.7%)	(2.0%, 14.1%)
Wet area	108.6	110.0	111.1

ACPD
10, 16007–16054, 2010

Table 5. Measured SNO_x for selected landcovers, classified by region (in $ng\,m^{-2}\,s^{-1}$).

ID	EUR	NAM	SAM	ASA	AFR
10	$4.40^{+5.38}_{-2.42}$	$3.62^{+7.14}_{-2.40}$			
11			$7.29^{+123.90}_{-6.88}$		$2.28^{+11.43}_{-1.90}$
12	$5.30^{+33.22}_{-4.57}$	$0.73^{+3.71}_{-0.61}$	$3.51^{+8.51}_{-2.48}$	$6.69^{+14.06}_{-4.54}$	$4.53^{+3.48}_{-1.97}$
13			$14.90^{+32.74}_{-10.24}$		$2.37^{+5.53}_{-1.66}$
16	$1.11^{+3.43}_{-0.84}$	$2.51^{+6.92}_{-1.84}$			
20			$2.49^{+11.26}_{-2.04}$	$1.36^{+1.92}_{-0.80}$	$2.02^{+1.79}_{-0.95}$
21	$2.47^{+29.07}_{-2.28}$	$6.06^{+19.45}_{-4.62}$	$2.55^{+13.55}_{-2.15}$	$6.35^{+23.87}_{-5.01}$	$15.21^{+19.40}_{-8.52}$

ACPD
10, 16007–16054, 2010

Table 6. Mean measured (number of measurements in brackets) and simulated (LC and YL95/SL10) SNO_x for each landcover type with measurements for the exactly corresponding yearly period.

ID	N	measured	LC	YL95/SL10
5	31(3)	$0.52^{+0.44}_{-0.24}$	0	$0.57^{+0.16}_{-0.12}$
6	220(20)	$0.74^{+2.25}_{-0.56}$	0	$0.77^{+0.32}_{-0.23}$
8	11(1)	0.03	$0.23^{+0}_{-0.04}$	$0.05^{+0.01}_{-0.01}$
10	242(22)	$3.28^{+5.04}_{-1.99}$	$0.27^{+0.41}_{-0.13}$	$3.49^{+2.67}_{-1.51}$
11	308(28)	$2.27^{+19.77}_{-2.04}$	$4.84^{+42.16}_{-2.08}$	$2.62^{+1.94}_{-1.11}$
12	1059(98)	$4.21^{+23.28}_{-3.57}$	$2.75^{+15.2}_{-1.31}$	$2.75^{+1.97}_{-1.15}$
13	99(9)	$7.85^{+23.84}_{-5.9}$	$3.1^{+9.41}_{-0.73}$	$8.03^{+2.9}_{-2.13}$
14	33(3)	$0.12^{+1.31}_{-0.11}$	$0.17^{+1.85}_{-0.09}$	$0.11^{+0.11}_{-0.06}$
16	227(22)	$1.11^{+3.29}_{-0.83}$	$0.1^{+0.28}_{-0.06}$	$1.09^{+1.62}_{-0.65}$
18	695(65)	$4.28^{+16.94}_{-3.42}$	$0.1^{+0.4}_{-0.07}$	$4.18^{+11.66}_{-3.08}$
19	77(7)	$0.97^{+1.54}_{-0.59}$	$0.77^{+1.22}_{-0.22}$	$0.8^{+0.35}_{-0.24}$
20	581(54)	$1.75^{+6.71}_{-1.39}$	$5.78^{+22.11}_{-1.88}$	$1.43^{+1.09}_{-0.62}$
21	2121(196)	$5^{+28.86}_{-4.27}$	$7.11^{+40.99}_{-6.05}$	$4.77^{+20.33}_{-3.86}$
All	5704(528)	$3.13^{+17.11}_{-2.65}$	$2.01^{+10.6}_{-1.77}$	$2.75^{+7.73}_{-2.03}$

ACPD
10, 16007–16054, 2010

Table 7. Adopted wet and dry emission factors of the soil biogenic NO emission algorithm based on the Yienger and Levy (1995) algorithm for the regions of Fig. 1 with the number of simulated points and measured points (in brackets).

LC	EUR		NAM		SAM		ASA		2AFR	
	wet	dry	wet	dry	wet	dry	wet	dry	wet	dry
5							$0.06^{+0.02}_{-0.02}$	$0.42^{+0.15}_{-0.11}$		
							31(3)			
6			$0.05^{+0.14}_{-0.04}$	$0.38^{+0.96}_{-0.27}$			$0.58^{+0.11}_{-0.10}$	$4.09^{+0.80}_{-0.67}$		
			209(19)				11(1)			
8			$0.01^{+0.00}_{-0.00}$	$0.05^{+0.01}_{-0.01}$						
			11(1)							
10	$1.28^{+1.43}_{-0.68}$	$9.47^{+10.60}_{-5.00}$	$0.63^{+1.17}_{-0.41}$	$4.58^{+8.41}_{-2.96}$						
	110(10)		132(12)							
11					$0.15^{+2.31}_{-0.14}$	$1.10^{+16.99}_{-1.04}$			$0.28^{+1.36}_{-0.23}$	$2.06^{+10.04}_{-1.71}$
					121(11)				187(17)	
12	$2.60^{+16.03}_{-2.24}$	$18.84^{+118.05}_{-16.25}$	$0.37^{+1.15}_{-0.28}$	$2.58^{+8.03}_{-1.95}$	$0.32^{+0.64}_{-0.21}$	$2.35^{+4.70}_{-1.57}$	$3.69^{+3.03}_{-1.66}$	$27.17^{+22.29}_{-12.24}$	$0.46^{+0.21}_{-0.15}$	$3.42^{+1.56}_{-1.07}$
	371(34)		314(29)		244(23)		97(9)		33(3)	
13					$0.79^{+0.21}_{-0.17}$	$6.66^{+1.78}_{-1.40}$			$0.30^{+0.47}_{-0.18}$	$2.58^{+3.97}_{-1.56}$
					44(4)				55(5)	
14	$0.20^{+0.56}_{-0.15}$	$1.50^{+4.08}_{-1.09}$	$0.00^{+0.00}_{-0.00}$	$0.01^{+0.00}_{-0.00}$						
	22(2)		11(1)							
16	$0.35^{+1.11}_{-0.27}$	$2.36^{+7.37}_{-1.79}$	$0.61^{+1.42}_{-0.42}$	$4.04^{+9.45}_{-2.83}$						
	172(17)		55(5)							
17	$1.38^{+6.49}_{-1.14}$	$9.80^{+46.67}_{-8.10}$			$0.54^{+0.05}_{-0.04}$	$3.96^{+0.35}_{-0.32}$				
	690(64)				11(1)					
19					$0.08^{+0.12}_{-0.05}$	$0.58^{+0.91}_{-0.36}$			$0.39^{+0.53}_{-0.22}$	$2.85^{+3.87}_{-1.64}$
					55(5)				22(2)	
20					$0.47^{+2.87}_{-0.41}$	$2.66^{+13.78}_{-2.23}$	$0.35^{+0.30}_{-0.16}$	$1.15^{+1.00}_{-0.54}$	$0.74^{+0.33}_{-0.23}$	$2.46^{+1.09}_{-0.75}$
					496(46)		52(5)		33(3)	
21	$0.23^{+1.86}_{-0.20}$	$1.58^{+13.02}_{-1.41}$	$0.33^{+0.45}_{-0.19}$	$2.31^{+3.17}_{-1.34}$	$0.28^{+1.09}_{-0.22}$	$1.94^{+7.65}_{-1.55}$	$0.72^{+2.22}_{-0.54}$	$5.03^{+15.57}_{-3.80}$	$1.28^{+1.04}_{-0.58}$	$8.96^{+7.31}_{-4.03}$

ACPD
10, 16007–16054, 2010

Table 8. Adopted wet and dry emission factors of the soil biogenic NO emission algorithm based on the Yienger and Levy (1995) algorithm for different duration classes of the measurement (<15, <30, <60, <90, <180, <365 days). The number of simulated points and measured points (in brackets) is given below the emission factors. If no additional measurements were performed in the next class, we left the field empty.

LC	=1	< 15	<30	<60	<90	<180	<365
5			$0.08^{+0.03}_{-0.02}$ $0.53^{+0.20}_{-0.15}$	$0.04^{+0.04}_{-0.02}$ $0.27^{+0.31}_{-0.14}$			
			11(1)	22(2)			
6			$0.04^{+0.10}_{-0.03}$ $0.28^{+0.70}_{-0.20}$	$0.04^{+0.12}_{-0.03}$ $0.31^{+0.86}_{-0.23}$		$0.05^{+0.14}_{-0.04}$ $0.38^{+0.96}_{-0.27}$	$0.09^{+0.31}_{-0.07}$ $0.63^{+2.18}_{-0.49}$
			66(6)	198(18)		209(19)	220(20)
8				$0.01^{+0.00}_{-0.00}$ $0.05^{+0.01}_{-0.01}$			
				11(1)			
10	$4.59^{+1.34}_{-1.04}$ $33.99^{+9.93}_{-7.68}$	$0.17^{+0.43}_{-0.12}$ $1.22^{+3.18}_{-0.88}$		$0.84^{+2.31}_{-0.61}$ $6.09^{+17.26}_{-4.50}$		$0.89^{+1.73}_{-0.59}$ $6.41^{+12.12}_{-4.19}$	$0.85^{+1.47}_{-0.54}$ $6.15^{+10.33}_{-3.86}$
	11(1)	22(2)		55(5)		231(21)	242(22)
11	$0.10^{+0.29}_{-0.07}$ $0.71^{+2.15}_{-0.53}$	$0.45^{+1.72}_{-0.36}$ $3.29^{+12.69}_{-2.61}$	$0.16^{+2.17}_{-0.15}$ $1.21^{+15.98}_{-1.12}$	$0.21^{+2.35}_{-0.19}$ $1.55^{+17.28}_{-1.42}$	$0.24^{+1.71}_{-0.21}$ $1.76^{+12.56}_{-1.54}$		
	33(3)	110(10)	220(20)	275(25)	308(28)		
12	$0.46^{+1.46}_{-0.35}$ $3.39^{+10.78}_{-2.58}$	$0.27^{+1.19}_{-0.22}$ $1.96^{+8.73}_{-1.60}$	$0.23^{+1.29}_{-0.19}$ $1.63^{+9.20}_{-1.38}$	$0.15^{+0.94}_{-0.13}$ $1.09^{+6.58}_{-0.93}$	$0.20^{+1.33}_{-0.18}$ $1.43^{+9.33}_{-1.24}$	$0.55^{+5.69}_{-0.50}$ $3.87^{+39.85}_{-3.53}$	$0.39^{+2.04}_{-0.33}$ $2.76^{+14.27}_{-2.31}$
	33(3)	187(17)	506(46)	682(62)	715(65)	803(73)	1009(93)
13	$0.11^{+0.10}_{-0.05}$ $0.90^{+0.88}_{-0.44}$	$1.00^{+3.31}_{-0.77}$ $8.51^{+28.03}_{-6.53}$	$0.63^{+1.05}_{-0.39}$ $5.34^{+8.87}_{-3.34}$	$0.67^{+0.75}_{-0.35}$ $5.68^{+6.32}_{-2.99}$	$0.35^{+0.58}_{-0.22}$ $2.97^{+4.88}_{-1.84}$		$0.62^{+0.57}_{-0.30}$ $5.28^{+4.82}_{-2.52}$
	22(2)	44(4)	55(5)	77(7)	88(8)		99(9)
14		$0.02^{+0.23}_{-0.01}$ $0.12^{+1.66}_{-0.11}$					
		33(3)					
16			$0.53^{+1.32}_{-0.38}$ $3.53^{+8.78}_{-2.52}$	$0.57^{+1.15}_{-0.38}$ $3.79^{+7.68}_{-2.54}$	$0.56^{+0.88}_{-0.34}$ $3.71^{+5.88}_{-2.27}$	$0.95^{+2.10}_{-0.65}$ $6.34^{+13.98}_{-4.36}$	$0.34^{+0.85}_{-0.24}$ $2.23^{+5.65}_{-1.60}$
			55(5)	66(6)	77(7)	88(8)	198(19)
17	$0.54^{+0.05}_{-0.04}$ $3.78^{+0.33}_{-0.30}$	$1.21^{+1.74}_{-0.71}$ $8.47^{+12.17}_{-4.99}$	$1.17^{+1.67}_{-0.69}$ $8.26^{+11.85}_{-4.87}$	$1.81^{+4.48}_{-1.29}$ $12.73^{+31.46}_{-9.06}$	$2.12^{+6.04}_{-1.57}$ $14.89^{+42.38}_{-11.02}$		$0.82^{+4.40}_{-0.69}$ $5.75^{+30.87}_{-4.84}$
	11(1)	198(18)	319(29)	550(50)	583(53)		683(63)
19	$0.39^{+0.53}_{-0.22}$ $2.85^{+3.87}_{-1.64}$	$0.17^{+0.16}_{-0.08}$ $1.21^{+1.18}_{-0.60}$	$0.08^{+0.14}_{-0.05}$ $0.62^{+1.03}_{-0.39}$				
	22(2)	66(6)	77(7)				
20	$0.48^{+2.45}_{-0.40}$ $1.58^{+8.11}_{-1.32}$	$0.54^{+1.05}_{-0.36}$ $2.72^{+6.84}_{-1.95}$	$0.73^{+0.64}_{-0.34}$ $2.65^{+2.55}_{-1.30}$	$1.65^{+3.38}_{-1.11}$ $6.60^{+19.01}_{-4.90}$	$2.49^{+4.69}_{-1.63}$ $12.29^{+35.69}_{-9.14}$	$1.32^{+2.45}_{-0.86}$ $7.22^{+13.56}_{-4.71}$	$0.66^{+1.43}_{-0.45}$ $3.50^{+6.67}_{-2.29}$
	55(5)	99(9)	132(12)	176(16)	198(18)	253(23)	561(52)
21	$0.92^{+9.24}_{-0.84}$ $6.46^{+64.65}_{-5.87}$	$0.47^{+3.97}_{-0.42}$ $3.29^{+27.79}_{-2.94}$	$0.27^{+3.53}_{-0.25}$ $1.87^{+24.71}_{-1.74}$	$0.50^{+2.93}_{-0.43}$ $3.50^{+20.54}_{-2.99}$	$0.69^{+2.82}_{-0.55}$ $4.83^{+19.71}_{-3.88}$	$0.58^{+3.26}_{-0.49}$ $4.03^{+22.85}_{-3.42}$	$0.55^{+2.46}_{-0.45}$ $3.86^{+17.19}_{-3.15}$
	110(10)	374(34)	605(55)	1133(103)	1397(127)	1803(164)	2037(187)

ACPD
10, 16007–16054, 2010

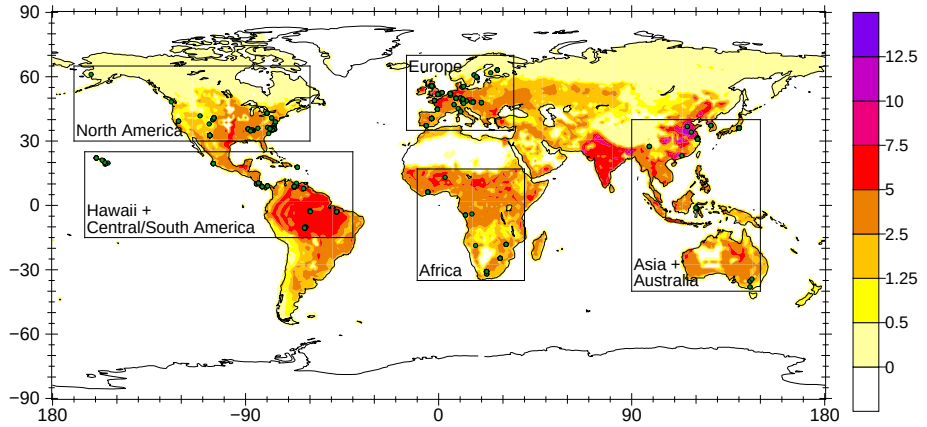

Fig. 1. SNO_x flux in the YL95e simulation (in ng m^{-2} s^{-1}), along with the locations of measurements (dots) and the regions referred to in Sect. 3.6.1.

ACPD
10, 16007–16054, 2010

Simulated biogenic soil NO emission improvement

J. Steinkamp and M. G. Lawrence

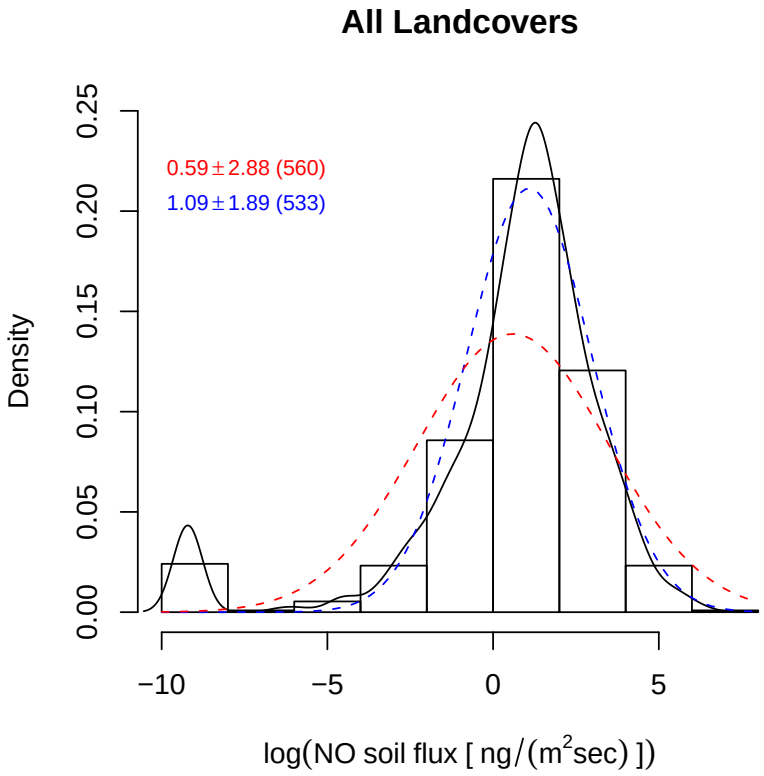

Fig. 2. Logarithmic histogram and probability density function of all measured SNO_x in the dataset. The blue dashed line represents the standard distribution with values ≤0 removed and the red dashed line represents the standard distribution with values ≤0 set to 10^{-4} (this results in the small peak at −9.2 (≈−4ln(10)) towards the left of the plot). In the upper left corner values are given for the mean, standard deviation and number of points (in brackets), respectively.

ACPD
10, 16007–16054, 2010

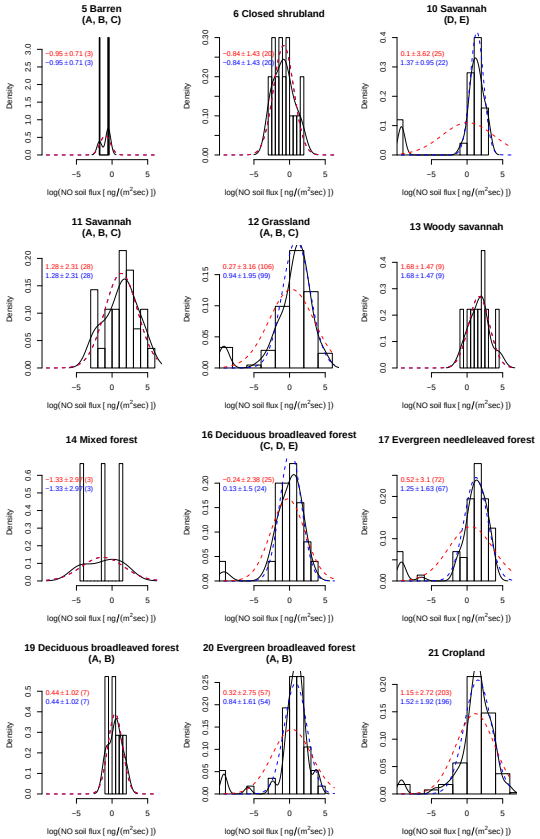

Fig. 3. Logarithmic histogram and probability density function per MODIS landcover and Koeppen main climate class (in brackets) of measured SNO_x in the dataset. The blue dashed line represents the standard distribution with values ≤0 removed and the red dashed line represents the standard distribution with values ≤0 set to 10^{-4}. The mean, standard deviation and numbers of measurements (in brackets) are in the upper left corner.

ACPD
10, 16007–16054, 2010

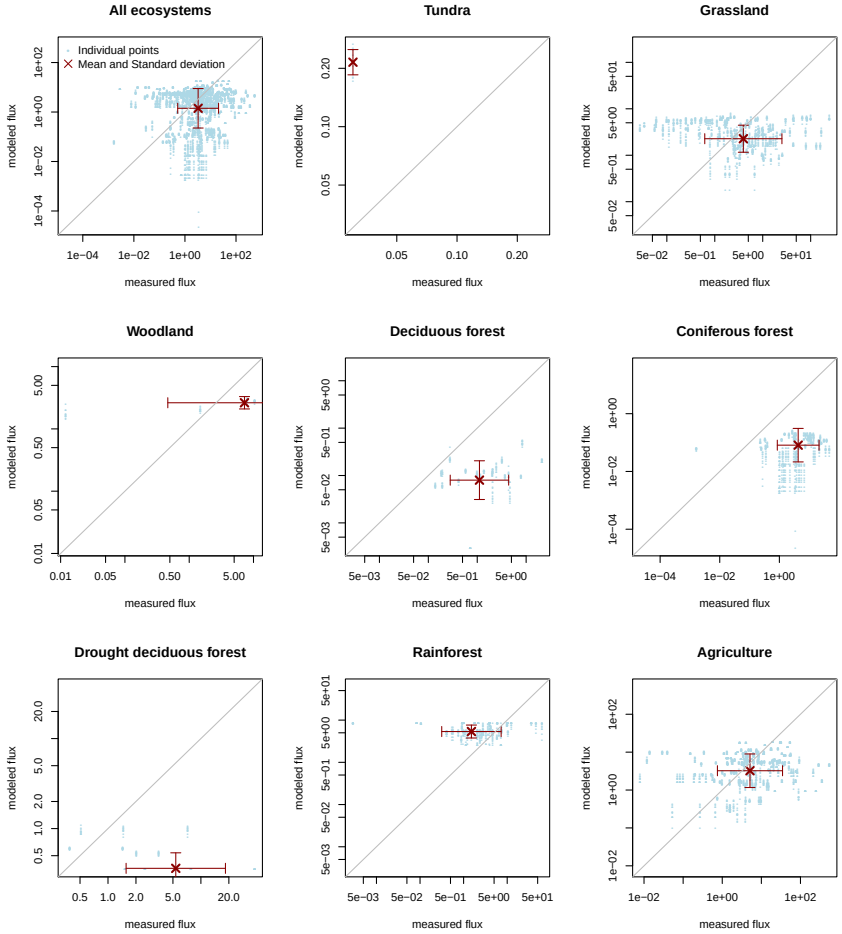

Fig. 4. Scatterplot of simulated SNO_x in YL95e for each corresponding period of the year versus each measurement along with the mean values and standard deviations.

ACPD
10, 16007–16054, 2010

Simulated biogenic soil NO emission improvement

J. Steinkamp and M. G. Lawrence

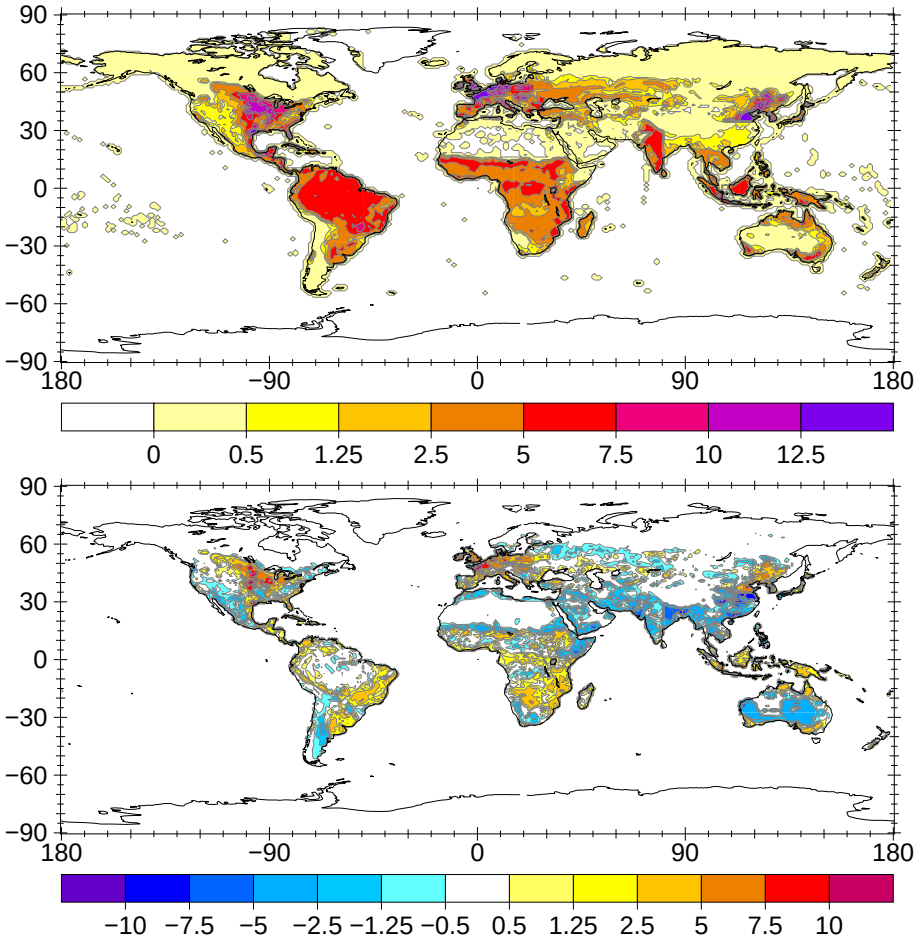

Fig. 5. Averaged SNO_x flux in the whole simulation period (in ng m^{-2} s^{-1}) for the LC simulation (upper panel) and the change compared to the YL95e simulation (lower panel).

ACPD
10, 16007–16054, 2010

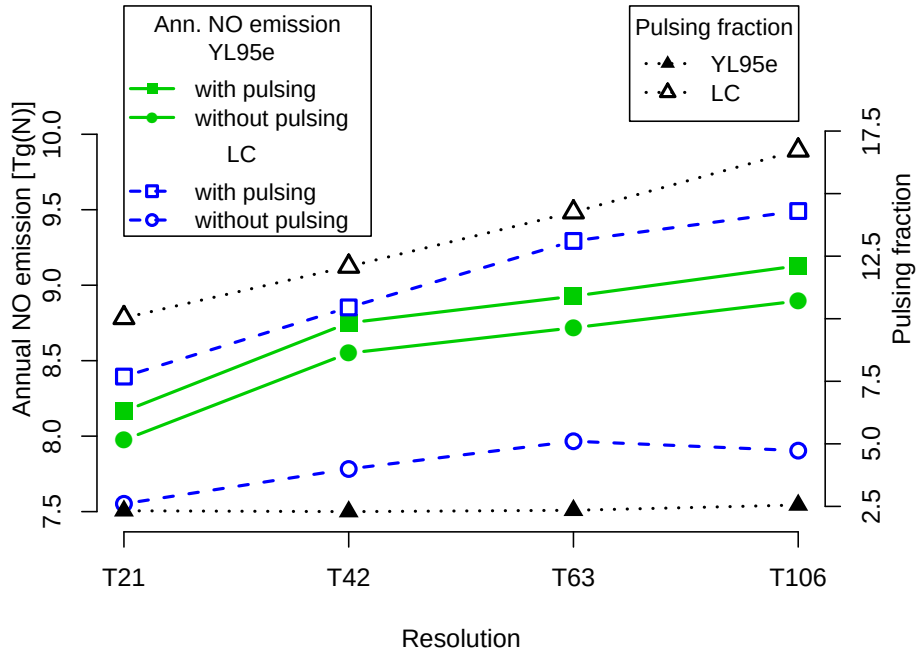

Fig. 6. Change of soil biogenic NO emission with pulsing (boxes), without (circles) and pulsing fraction (triangles) for the YL95e simulation (filled) and the LC simulation (outlined) at four different horizontal resolutions.

ACPD
10, 16007–16054, 2010

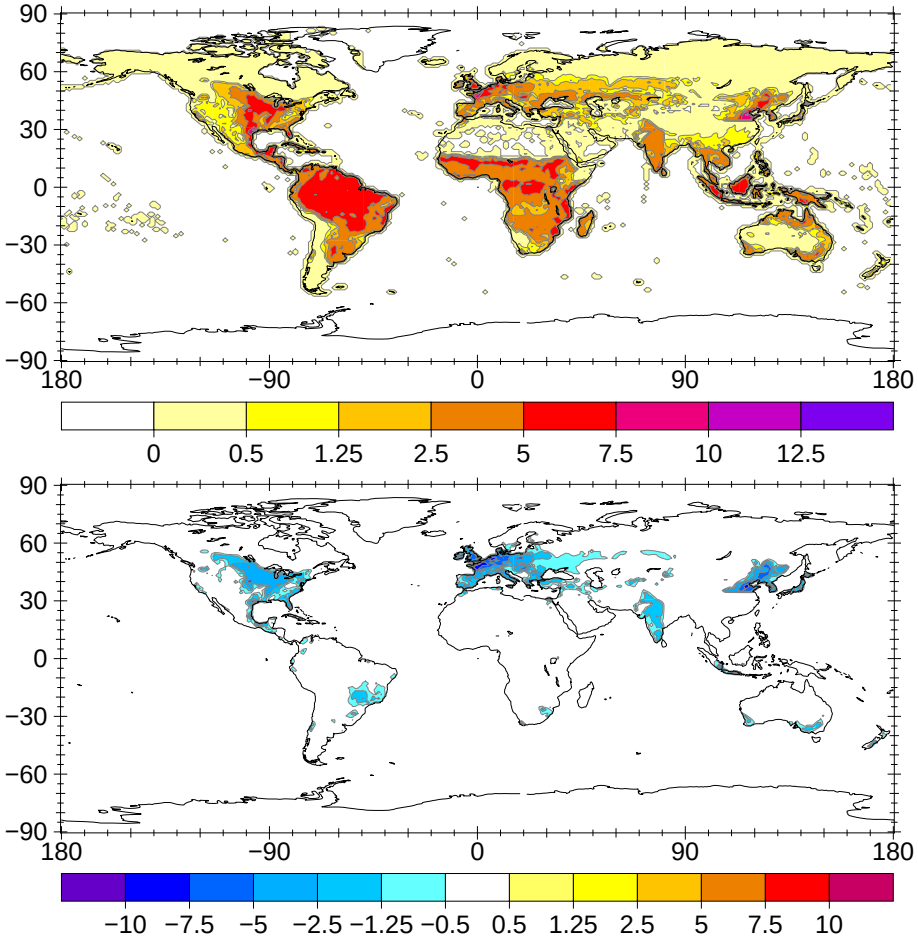

Fig. 7. Averaged SNO_x flux in the whole simulation period (in $ng\,m^{-2}\,s^{-1}$) for the LC+FIE simulation (upper panel) and the change compared to the LC simulation (lower panel).

ACPD
10, 16007–16054, 2010

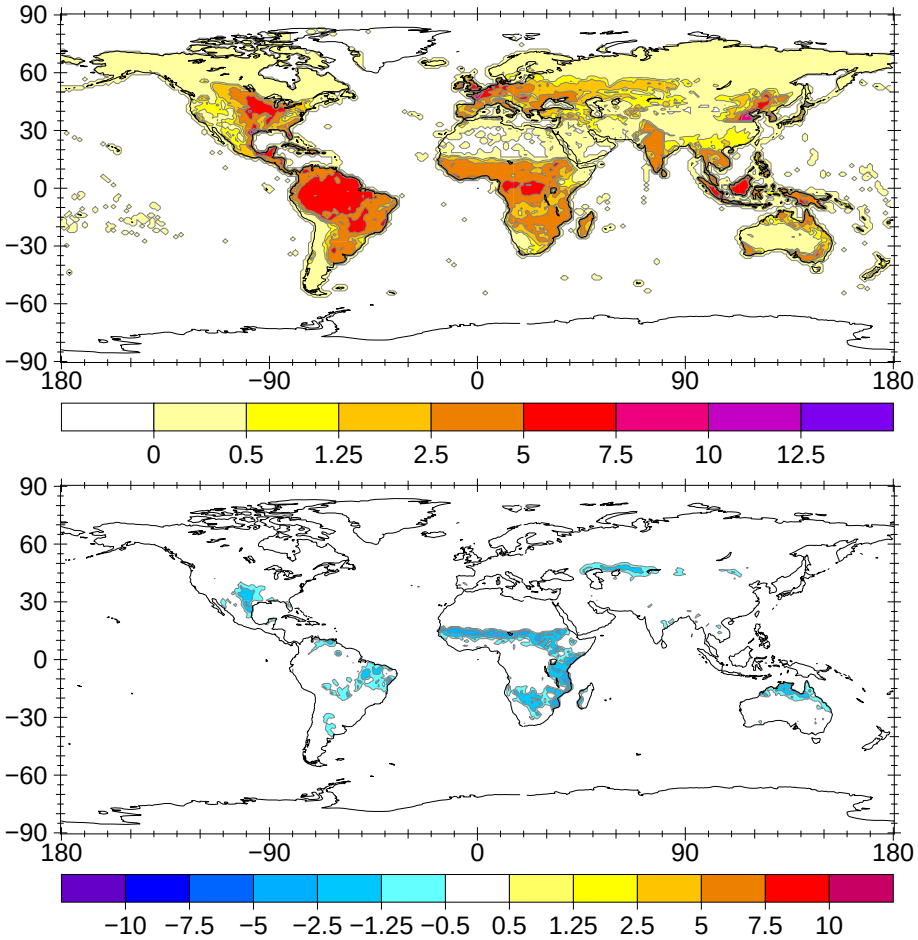

Fig. 8. Averaged SNO_x flux in the whole simulation period (in $ng\,m^{-2}\,s^{-1}$) for the LC+FIE+VSM simulation (upper panel) and the change compared to the LC+FIE simulation (lower panel).

ACPD
10, 16007–16054, 2010

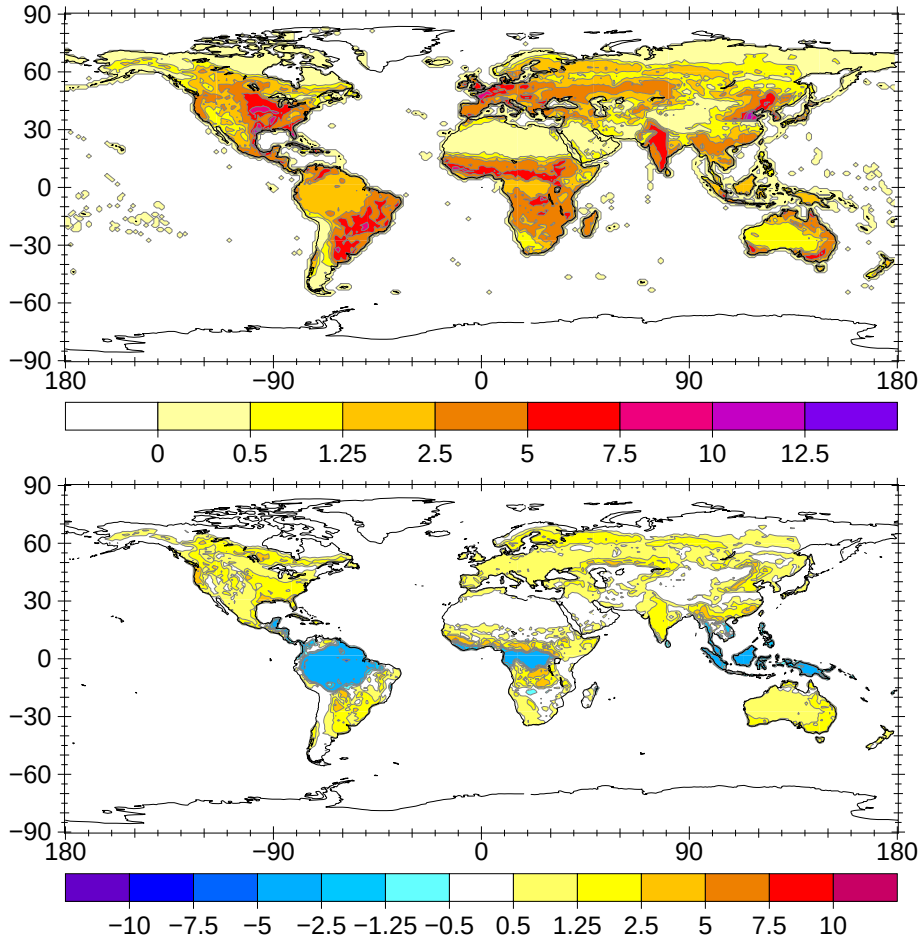

Fig. 9. Averaged SNO_x flux in the whole simulation period (in $ng\,m^{-2}\,s^{-1}$) for the YL95/SL10 simulation (upper panel) and the change compared to the LC+FIE+VSM simulation (lower panel).

ACPD
10, 16007–16054, 2010

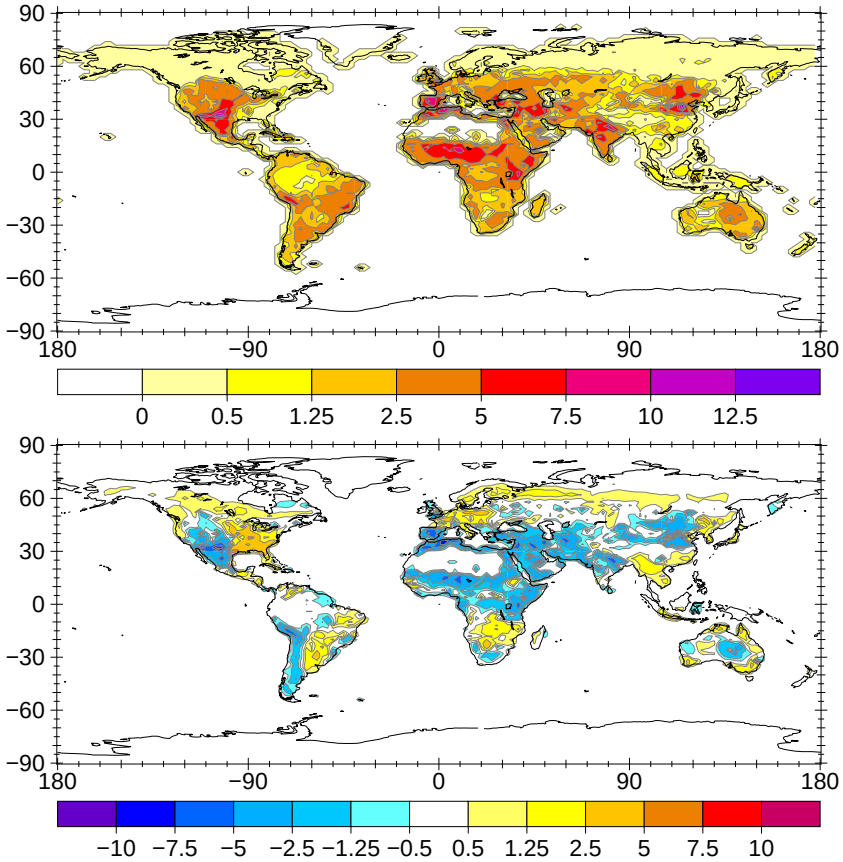

Fig. 10. Averaged SNO_x flux for the year 2000 of the Jaeglé et al. (2005) (J05) inverse modeling study (in $ng\,m^{-2}\,s^{-1}$) (upper panel) and the difference (YL95/SL10–J05) to the flux of the YL95/SL10 year 2000 simulation (lower panel).

ACPD
10, 16007–16054, 2010

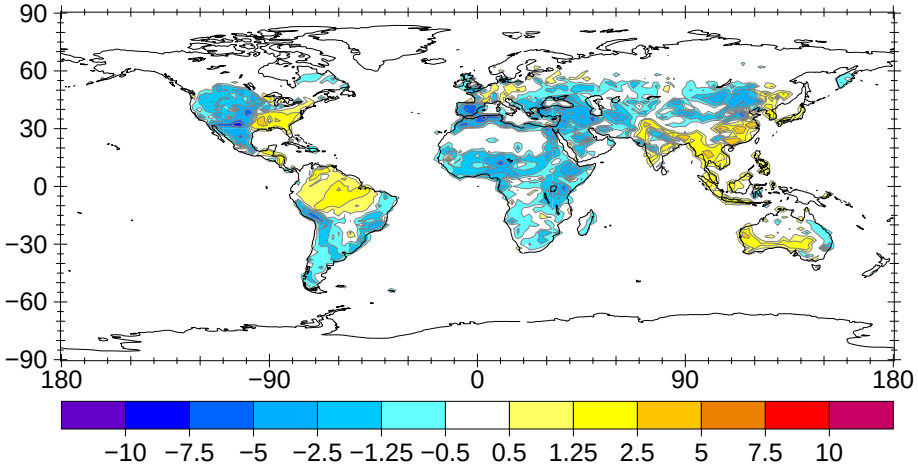

Fig. 11. Difference between YL95e and Jaeglé et al. (2005) (J05) (YL95/SL10–J05) (in $\mathrm{ng\,m^{-2}\,s^{-1}}$) for the year 2000.

ACPD
10, 16007–16054, 2010

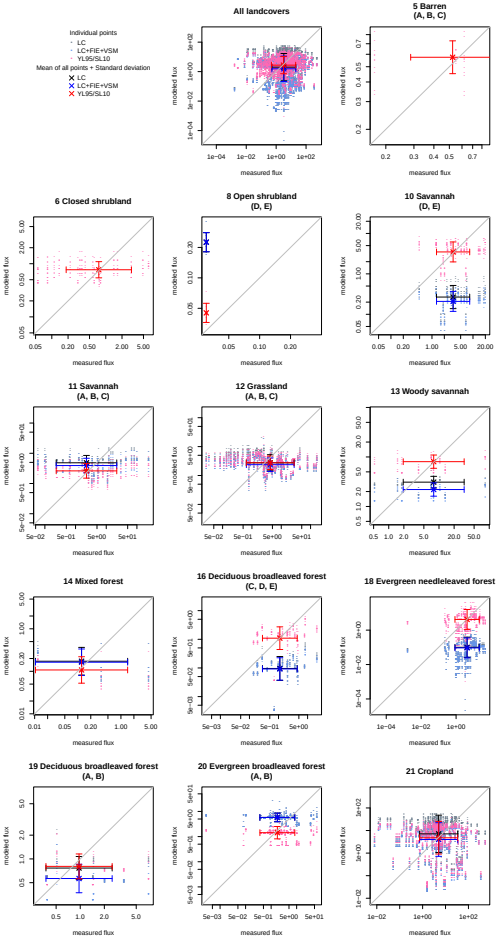

Fig. 12. Scatterplots of SNO_x measurements versus model results for the YL95/SL10 simulations.

ACPD
10, 16007–16054, 2010

Simulated biogenic soil NO emission improvement

J. Steinkamp and M. G. Lawrence

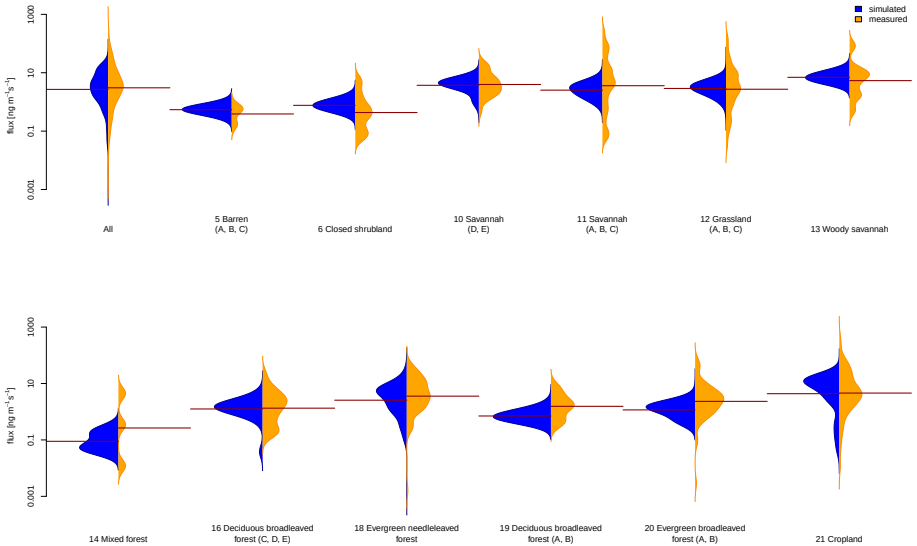

Fig. 13. Density function plot of SNO_x measurements (orange) versus model output (blue) for the YL95/SL10 simulation using the program by Kampstra (2008).

ACPD
10, 16007–16054, 2010